

UC Berkeley

UC Berkeley Previously Published Works

Title

The Lick Observatory Supernova Search follow-up program: photometry data release of 70 SESNe

Permalink

<https://escholarship.org/uc/item/08c0r6qq>

Journal

Monthly Notices of the Royal Astronomical Society, 512(3)

ISSN

0035-8711

Authors

Zheng, WeiKang

Stahl, Benjamin E

de Jaeger, Thomas

et al.

Publication Date

2022-03-31

DOI

10.1093/mnras/stac723

Peer reviewed

The Lick Observatory Supernova Search follow-up program: photometry data release of 70 stripped-envelope supernovae

WeiKang Zheng,^{1*} Benjamin E. Stahl,^{1,2} Thomas de Jaeger,^{1,3} Alexei V. Filippenko,^{1,4} Shan-Qin Wang,⁵ Wen-Pei Gan,⁵ Thomas G. Brink,¹ Ivan Altunin,¹ Raphael Baer-Way,¹ Andrew Bigley,¹ Kyle Blanchard,¹ Peter K. Blanchard,⁶ James Bradley,¹ Samantha K. Cargill,¹ Chadwick Casper,¹ Teagan Chapman,¹ Vidhi Chander,¹ Sanyum Channa,^{2,7} Byung Yun Choi,¹ Nick Choksi,¹ Matthew Chu,² Kelsey I. Clubb,¹ Daniel P. Cohen,⁸ Paul A. Dalba,^{9,10} Asia deGraw,¹ Maxime de Kouchkovsky,¹ Michael Ellison,¹ Edward Falcon,¹ Ori D. Fox,¹¹ Kiera Fuller,¹ Mohan Ganeshalingam,¹² Nachiket Girish,² Carolina Gould,¹ Goni Halevi,^{1,13} Andrew Halle,¹ Kevin T. Hayakawa,⁸ Romain Hardy,⁸ Julia Hestenes,¹ Andrew M. Hoffman,¹ Michael Hyland,¹ Benjamin T. Jeffers,¹ Connor Jennings,¹ Michael T. Kand rashoff,¹ Anthony Khodanian,¹ Minkyu Kim,¹ Haejung Kim,¹ Michelle E. Kislay,^{1,14} Daniel Krishnan,¹ Sahana Kumar,^{1,15} Snehaa Ganesh Kumar,¹ Joel Leja,^{16,17,18} Erin J. Leonard,^{1,19} Gary Z. Li,²⁰ Weidong Li,^{1†} Ji-Shun Lian,⁵ Evelyn Liu,¹ Thomas B. Lowe,³ Philip Lu,²¹ Emily Ma,¹ Michelle N. Mason,²² Michael May,¹ Kyle McAllister,¹ Emma McGinness,¹ Shaunak Modak,^{2,13} Jeffrey Molloy,¹ Yupei S. Murakami,²³ Omnarayani Nayak,¹¹ Derek Perera,¹ Kenia Pina,¹ Druv Punjabi,¹ Andrew Rikhter,²⁴ Timothy W. Ross,¹ Jackson Sipple,¹ Costas Soler,¹ Samantha Stegman,^{1,25} Haynes Stephens,¹ James Sunseri,^{1,2} Kevin Tang,¹ Stephen Taylor,¹ Patrick Thrasher,¹ Schuyler D. Van Dyk,²⁶ Xiang-Gao Wang,⁵ Jeremy Wayland,¹ Andrew Wilkins,¹ Abel Yagubyan,¹ Heechan Yuk,²⁷ Sameen Yunus,¹ and Keto D. Zhang¹

¹Department of Astronomy, University of California, Berkeley, CA 94720-3411, USA

²Department of Physics, University of California, Berkeley, CA 94720-7300, USA

³Institute for Astronomy, University of Hawaii, 2680 Woodlawn Drive, Honolulu, HI 96822, USA

⁴Miller Institute for Basic Research in Science, University of California, Berkeley, CA 94720, USA

⁵Guangxi Key Laboratory for Relativistic Astrophysics, School of Physical Science and Technology, Guangxi University, Nanning 530004, China

⁶Center for Interdisciplinary Exploration and Research in Astrophysics (CIERA) and Department of Physics and Astronomy, Northwestern University, 1800 Sherman Ave., Evanston, IL 60201, USA

⁷Department of Physics, Stanford University, Stanford, CA 94305, USA

⁸Department of Physics and Astronomy, University of California, Los Angeles, CA 90095, USA

⁹Department of Astronomy and Astrophysics, University of California Santa Cruz, 1156 High St., Santa Cruz, CA 95064, USA

¹⁰Department of Earth and Planetary Sciences, University of California Riverside, 900 University Ave., Riverside, CA 92521, USA

¹¹Space Telescope Science Institute, 3700 San Martin Drive, Baltimore, MD 21218, USA

¹²Lawrence Berkeley National Laboratory, 1 Cyclotron Rd, Berkeley, CA 94720, USA

¹³Department of Astrophysical Sciences, Princeton University, 4 Ivy Lane, Princeton, NJ 08544, USA

¹⁴Netflix, Inc., 100 Winchester Cir, Los Gatos, CA 95032, USA

¹⁵Department of Physics, Florida State University, Tallahassee, FL 32306, USA

¹⁶Department of Astronomy & Astrophysics, The Pennsylvania State University, University Park, PA 16802, USA

¹⁷Institute for Computational & Data Sciences, The Pennsylvania State University, University Park, PA, USA

¹⁸Institute for Gravitation and the Cosmos, The Pennsylvania State University, University Park, PA 16802, USA

¹⁹Jet Propulsion Laboratory, California Institute of Technology, Pasadena, CA 91109, USA

²⁰The Aerospace Corporation, 2310 E. El Segundo Blvd., El Segundo, CA, 90245, USA

²¹Center for Theoretical Physics, Department of Physics and Astronomy, Seoul National University, Seoul 08826, Korea

²²Department of Physics and Astronomy, University of Wyoming, 1000 E. University, Dept. 3905, Laramie, WY 82071, USA

²³Department of Physics and Astronomy, Johns Hopkins University, Baltimore, MD 21218, USA

²⁴Department of Physics, University of California San Diego, La Jolla, CA 92093, USA

²⁵Argonne National Laboratory, 9700 S. Cass Avenue, Lemont, IL 60439, USA

²⁶Caltech/Spitzer Science Center, Caltech/IPAC, Mailcode 100-22, Pasadena, CA 91125, USA

²⁷Department of Physics and Astronomy, University of Oklahoma, 440 W. Brooks St., Norman, OK 73019, USA

ABSTRACT

We present *BVRI* and unfiltered (*Clear*) light curves of 70 stripped-envelope supernovae (SESNe), observed between 2003 and 2020, from the Lick Observatory Supernova Search (LOSS) follow-up program. Our SESN sample consists of 19 spectroscopically normal SNe Ib, two peculiar SNe Ib, six SNe Ibn, 14 normal SNe Ic, one peculiar SN Ic, ten SNe Ic-BL, 15 SNe IIb, one ambiguous SN IIb/Ib/c, and two superluminous SNe. Our follow-up photometry has (on a per-SN basis) a mean coverage of 81 photometric points (median of 58 points) and a mean cadence of 3.6 d (median of 1.2 d). From our full sample, a subset of 38 SNe have pre-maximum coverage in at least one passband, allowing for the peak brightness of each SN in this subset to be quantitatively determined. We describe our data collection and processing techniques, with emphasis toward our automated photometry pipeline, from which we derive publicly available data products to enable and encourage further study by the community. Using these data products, we derive host-galaxy extinction values through the empirical colour evolution relationship and, for the first time, produce accurate rise-time measurements for a large sample of SESNe in both optical and infrared passbands. By modeling multiband light curves, we find that SNe Ic tend to have lower ejecta masses and lower ejecta velocities than SNe Ib and IIb, but higher ⁵⁶Ni masses.

Key words: galaxies: distances and redshifts – supernovae: general

1 INTRODUCTION

It is well established that massive stars (i.e., those having $M \gtrsim 8 M_{\odot}$) have short lives that end in catastrophic explosions known as core-collapse supernovae (CCSNe). Among CCSNe, those whose spectra show features of hydrogen are classified as Type II SNe (see, e.g., Filippenko 1997; Gal-Yam 2017 for reviews of SN classification). In contrast, hydrogen-poor CCSNe are classified as Type Ib or Ic, depending on whether their optical spectra contain obvious helium features (Matheson 2001). The progenitor stars of hydrogen-poor CCSNe have their outer envelopes stripped away before explosion by strong winds during the Wolf-Rayet phase (e.g., Conti 1975; Smith & Owocki 2006; Gal-Yam et al. 2014). By interaction with a binary companion (e.g., Podsiadlowski et al. 1992; Sana et al. 2012; Eldridge et al. 2013), or some combination of these two modes. If the envelope-stripping process is highly efficient, the helium shell is also removed before explosion, leading to the differentiation between SNe Ib (He-rich) and SNe Ic (He-poor). Hydrogen-poor CCSNe are generally referred to as stripped-envelope supernovae (SESNs).

SESNs are found to be observationally heterogeneous. For example, in some cases, the stripping process is incomplete and thus the envelope is left with some fraction of hydrogen. These SNe typically show H lines at early times that rapidly disappear after maximum light (Filippenko 1988; Filippenko et al. 1993), and their spectra resemble SNe Ib at late times. A small subset of SN Ib-like events show evidence of interaction with dense circumstellar material (CSM); having relatively narrow spectral emission lines (e.g., Pastorello et al. 2007; Foley et al. 2007; Hosseinzadeh et al. 2017), these objects have been dubbed SNe Ibn (“n” for “narrow lines”). In addition, a subset of SNe Ic characterised by the presence broad spectral lines which indicate extremely high ejecta velocities ($\gtrsim 15,000 \text{ km s}^{-1}$) are designated as SNe Ic-BL (e.g., Modjaz et al. 2014). Objects within this subclass have been found to be associated with long-duration gamma-ray bursts (e.g., Woosley & Bloom

2006). Recently, a new class, SNe Icn, has been proposed by Gal-Yam et al. (2021) based on the prototype SN 2019hgp, followed by SNe 2021csp (Perley et al. 2021; Fraser et al. 2021) and 2021ckj (Pastorello et al. 2021). The early-time spectra of these objects are dominated by narrow lines with profiles similar to those seen in SNe Ibn, but originating from carbon and oxygen rather than He. In any case, all of the aforementioned SN classifications (Ib, IIb, Ibn, Ic, Ic-BL, and Icn) are, to some extent, related to the envelope of their progenitor star being stripped. Accordingly, we consider all of them to be SESNe in the analysis presented herein.

Owing to the efforts of various SN surveys spanning the globe, the study of SESNe with large light-curve samples has proliferated. Li et al. (2011) presented a set of roughly two dozen unfiltered SESN light curves within $\sim 60 \text{ Mpc}$. In the same year, Drout et al. (2011) presented *V*- and *R*-band light curves of 25 SESNe from the Palomar 60 inch telescope. Bianco et al. (2014) published multiband light curves of 64 SESNe obtained by the Harvard-Smithsonian Center for Astrophysics (CfA) SN group, and Taddia et al. (2015) presented expanded sets of multiband light curves of 20 SESNe from the Sloan Digital Sky Survey (SDSS) SN Survey II. In addition, Stritzinger et al. (2018a) published 34 SESN light curves from the first phase of the Carnegie Supernova Project (CSP-I). Despite these impressive efforts, the state of large-scale photometric studies of SESNe substantially lags that of other SNe (e.g., SNe Ia, which are routinely studied photometrically at the hundreds-of-objects scale).

Over the past two decades, our Lick Observatory Supernova Search (LOSS; Filippenko et al. 2001) program has invested considerably in both discovering and monitoring all kinds of SNe, including SESNe. Large light-curve samples have already been published by Ganeshalingam et al. (2010) and Stahl et al. (2019) for SNe Ia, and by de Jaeger et al. (2019) for SNe II. In this paper, we release the light curves of 70 SESNe observed by LOSS since 2003. In the remainder of the paper, we describe the sample (Sec. 2) and our data-reduction strategies (Sec. 3) before presenting an analysis of the light curves (Sec. 4) and offering our conclusions (Sec. 5).

* E-mail: weikang@berkeley.edu; benjamin_stahl@berkeley.edu; tdejaeger@berkeley.edu; afilippenko@berkeley.edu; shanqin-wang@gxu.edu.cn
† Deceased 2011 December 12

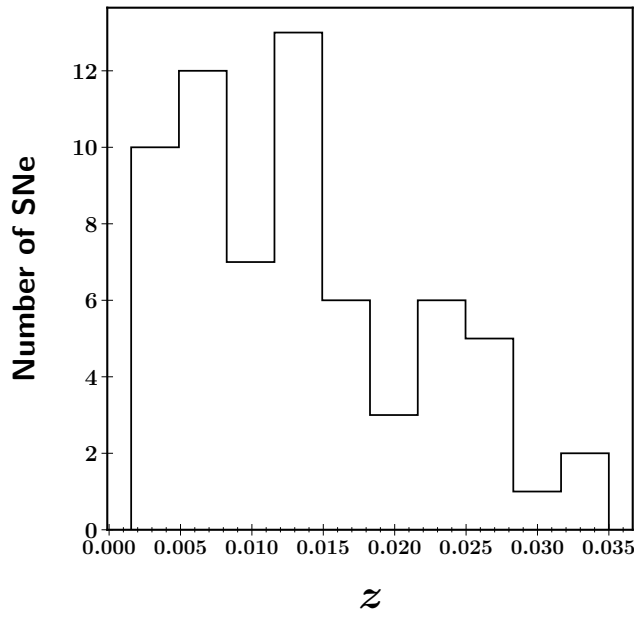


Figure 1. The redshift distribution of the 65 (out of 70 in total) SESNe in our sample which have reliable heliocentric velocity measurements from their host galaxies. The average redshift value is 0.0136 with a standard deviation of 0.0082, and 40 SESNe have $z > 0.01$.

2 DATA SAMPLE

The Berkeley SESN sample consists of 70 objects observed between 2003 and 2020. Two main telescopes were used for follow-up observations: (i) the fully robotic 0.76 m Katzman Automatic Imaging Telescope (KAIT; Filippenko et al. 2001), and (ii) the 1 m Anna Nickel telescope, both located at Lick Observatory on Mount Hamilton, near San Jose, CA, USA. Most SESNe in our sample were observed in multiple optical passbands (B, V, R, I), and some have additional *Clear-band* (unfiltered) data.¹ For a large fraction of SESNe in our sample, spectra were also obtained by our group using multiple facilities. A detailed analysis and release of the LOSS spectra of SESNe was published by Shivvers et al. (2019), so the present paper focuses exclusively on our photometric observations.

Table 1 provides the basic information for each SN in our sample, including its spectroscopic classification, host-galaxy name, distance, recession velocity, and Galactic extinction (Schlafly & Finkbeiner 2011). The listed classifications are adopted from the Transient Name Server² (TNS), but where they conflict with those given by Shivvers et al. (2019), we adopt the latter owing to the more sophisticated and systematic approach that resulted in their determinations. The single exception to this paradigm is SN 2008fz, which was classified as an SN Ic by Shivvers et al. (2019) but for which we adopt the classification of superluminous SN IIn (i.e., SLSN-IIIn) from Drake et al. (2010). In summary, our SESN sample consists of 19 spectroscopically normal SNe Ib, two peculiar SNe Ib, six SNe Ibn, 14 normal SNe Ic, one peculiar SN Ic, ten SNe Ic-BL, 15 SNe IIb, one ambiguous SN IIb/Ib/c, and two SLSNe.

The host-galaxy distances reported in Table 1 were obtained from the NASA/IPAC Extragalactic Database of redshift-

independent distances (NED-D³) when available, and otherwise calculated using a standard cosmological model with $H_0 = 70 \text{ km s}^{-1} \text{ Mpc}^{-1}$, $\Omega_M = 0.30$, and $\Omega_\Lambda = 0.70$. Figure 1 shows the redshift distribution of the 65 SESNe in our sample which have reliable host-galaxy heliocentric velocity measurements. The redshifts range from 0.0015 (SN 2011dh) to 0.0350 (SN 2009er), with an average value of 0.0136 and a standard deviation of 0.0082. 40 SESNe have $z > 0.01$. For the remaining five SESNe without host heliocentric velocity measurements, we adopt redshifts from various literature sources (see the footnote of Table 1 for more details).

3 DATA REDUCTION

All photometric data published herein were obtained with the Lick KAIT and 1 m Nickel telescopes. Over the past two decades, the KAIT CCD and filter have been updated several times, resulting in four different CCD/filter combinations, which we refer as KAIT1-4 (see Ganeshalingam et al. 2010; Stahl et al. 2019 for more details). In its current configuration (KAIT4), KAIT is equipped with a Finger Lakes Instrument camera with 512×512 pixels covering a 6.7×6.7 field of view. The 1 m Nickel is a human-operated telescope, but it can be remotely operated from the UC Berkeley campus. It is equipped with a thinned, Loral, 2048×2048 pixel CCD (binned by a factor of two along both axes to reduce the readout time), and has a 6.3×6.3 field of view. The filter set on the Nickel telescope was updated once, in March 2009; we refer to the configuration before and after this change as Nickel1 and Nickel2, respectively (again, see Ganeshalingam et al. 2010; Stahl et al. 2019 for more details).

A novel automated photometry pipeline⁴ was developed by Stahl et al. (2019) to process the significant volume of SN observations produced by LOSS consistently and accurately, while at the same time requiring minimal human intervention. Although we defer the details to Stahl et al. (2019), we briefly summarise the main procedures here. All images are first treated to remove the bias level, and are then flat-fielded before being astrometrically calibrated using code provided by astrometry.net⁵ (Lang et al. 2010). Where necessary, image subtraction is applied so as to remove host-galaxy contamination, with the template images being sourced on dark nights using the Nickel telescope after the SNe have faded beyond detection (generally > 6 months after discovery). Point-spread-function (PSF) photometry is obtained using DAOPHOT (Stetson 1987) from the IDL Astronomy User's Library⁶. Nearby stars are chosen from the Pan-STARRS1⁷ catalogue for calibration. Their magnitudes are first transformed into the Landolt system (Landolt 1983, 1992) using the empirical prescription (Eq. 6) presented by Tonry et al. (2012), and then transformed to the appropriate KAIT/Nickel natural system (i.e., KAIT1-4 or Nickel1-2 as appropriate based on the equipment configuration on the date of observation). All apparent magnitudes are measured in the natural system, and the final results are then transformed to the standard system (see Eqs. 1a–1d of Stahl et al. 2019) using local calibrators and the appropriate colour terms as given by Ganeshalingam et al. (2010) and Stahl et al. (2019). Note that when transforming from the natural system back to the standard system, there are additional errors associated with the transformation that are not accounted for

³ <http://ned.ipac.caltech.edu/Library/Distances/>

⁴ <https://github.com/benstahl192/LOSSPhotPipeline>

⁵ <https://astrometry.net>

⁶ <http://idlastro.gsfc.nasa.gov/>

⁷ <http://archive.stsci.edu/panstarrs/search.php>

¹ A small fraction are covered with only *Clear-band* observations.

² www.wis-tns.org

owing to differences between the spectral energy distributions of SNe and the reference stars (e.g., [Stritzinger et al. 2005](#)).

Table 1. SESN sample

SN	Type	RA (h,m,s) (J2000)	Dec.(°,′,″) (J2000)	Discovery Date (UT)	Host galaxy	A_V (MW)	Distance (Mpc)	Error (Mpc)	V_{helio}^1 (host) (km s $^{-1}$)	Error (km s $^{-1}$)	Subtraction $^{2?}$
2003gk	Ib	23:01:42.989	+02:16:08.69	2003-07-01	NGC 7460	0.24	48.2	28.0	3,192	7	Y
2006el	IIb	22:47:38.50	+39:52:27.59	2006-08-25	UGC 12188	0.31	—	—	5,115	14	Y
2006ep	Ib	00:41:24.88	+25:29:46.72	2006-08-30	NGC 214	0.10	51.1	12.3	4,537	4	N
2006jc	Ibn	09:17:20.78	+41:54:32.69	2006-10-09	UGC 4904	0.06	—	—	1,670	4	Y
2006lc	Ibn	22:44:24.45	-00:09:53.89	2006-10-21	NGC 7364	0.18	70.6	22.1	4,865	5	Y
2007C	Ib	13:08:49.30	-06:47:01.00	2007-01-07	NGC 4981	0.12	22.7	3.1	1,680	4	Y
2007D	Ic-BL	03:18:38.71	+37:36:26.39	2007-01-09	UGC 2653	0.92	103.8	5.6	6,939	5	Y
2007ag	Ib	10:01:35.99	+21:36:42.01	2007-03-07	UGC 5392	0.08	114.8	1.7	6,209	4	Y
2007cl	Ic	17:48:21.19	+54:09:05.18	2007-05-23	NGC 6479	0.12	—	—	6,650	43	Y
2007kj	Ib	00:01:19.58	+13:06:30.60	2007-10-02	NGC 7803	0.22	—	—	5,366	6	Y
2007ru	Ic-BL	23:07:23.14	+43:35:33.68	2007-11-27	UGC 12381	0.71	—	—	4,636	6	N
2007rw	IIb	12:38:03.64	-02:15:40.10	2007-11-29	UGC 7798	0.09	—	—	2,568	5	Y
2007rz	Ic	04:31:10.84	+07:37:51.49	2007-12-08	NGC 1590	0.55	—	—	3,897	7	Y
2007uy	Ib-pec	09:09:35.35	+33:07:08.90	2007-12-31	NGC 2770	0.06	28.7	4.2	1,947	2	Y
2008aq	IIb	12:50:30.42	-10:52:01.42	2008-02-27	MCG -02-33-20	0.12	32.0	3.0	2,390	5	N
2008cw	IIb	16:32:38.27	+41:27:33.19	2008-06-01	SDSS J163238.15+412730.8	0.02	—	—	9,726	25	Y
2008dq	Ic	16:06:03.11	+55:25:37.42	2008-06-25	UGC 10214	0.03	—	—	9,401	15	Y
2008eb	Ib	18:11:52.17	+14:58:50.59	2008-07-07	NGC 6574	0.48	33.7	7.2	2,282	5	Y
2008ew	Ic	16:58:28.92	+20:02:38.00	2008-08-10	IC 1236	0.22	38.0	—	6,030	5	Y
2008fi	IIb	01:53:23.17	+29:21:28.40	2008-08-26	SDSS J015322.95+292131.2	0.17	—	—	—	—	N
2008fz	SLSN-IIIn	23:16:16.60	+11:42:47.48	2008-09-22	Anon.	0.12	—	—	—	—	N
2008gj	Ic	22:36:28.57	+21:37:55.31	2008-10-19	NGC 7321	0.13	92.0	10.9	7,145	5	Y
2009C	IIb	23:13:42.84	+49:40:47.21	2009-01-02	UGC 12433	0.79	—	—	6,985	32	Y
2009K	IIb	04:36:36.77	-00:08:35.59	2009-01-14	NGC 1620	0.16	40.2	4.7	3,512	1	Y
2009Z	IIb	14:01:53.61	-01:20:30.19	2009-02-02	SDSS J140153.80-012035.5	0.13	—	—	7,534	3	N
2009er	Ib-pec	15:39:29.84	+24:26:05.32	2009-05-22	SDSS J153930.49+242614.8	0.12	—	—	10,492	67	N
2009gk	IIb	21:44:27.28	+14:53:57.30	2009-06-23	UGC 11803	0.24	—	—	7,946	34	Y
2009hy	Ic	22:16:27.02	+16:28:13.01	2009-08-02	NGC 7244	0.14	—	—	7,564	7	Y
2009jf	Ib	23:04:52.98	+12:19:59.48	2009-09-27	NGC 7479	0.31	28.3	6.1	2,381	1	Y
2010cn	IIb	11:04:06.57	+04:49:58.69	2010-05-04	SDSS J110406.40+044955.5	0.13	—	—	7,795	—	Y
2010gd	Ic	17:57:40.98	+27:49:48.11	2010-07-08	UGC 11064	0.16	107.1	21.6	7,043	10	Y
2010hy	SLSN-I	18:59:32.89	+19:24:25.88	2010-09-04	Anon.	1.45	—	—	—	—	N
2011dh	IIb	13:30:05.12	+47:10:10.81	2011-06-01	NGC 5194	0.10	7.2	2.1	463	3	Y
2011fu	IIb	02:08:21.41	+41:29:12.30	2011-09-21	UGC 1626	0.21	—	—	5,543	11	Y
2011gd	Ib	16:34:25.67	+21:32:28.39	2011-08-28	NGC 6186	0.13	—	—	2,937	29	Y
2012aa	Ic	14:52:33.48	-03:31:54.01	2012-01-29	Anon.	0.28	—	—	—	—	Y
2012ap	Ic-BL	05:00:13.72	-03:20:51.22	2012-02-10	NGC 1729	0.14	39.3	3.3	3,632	4	N

Table 1 (cont'd)

SN	Type	RA (h,m,s) (J2000)	Dec.(°,′,″) (J2000)	Discovery Date (UT)	Host galaxy	A_V (MW)	Distance (Mpc)	Error (Mpc)	V_{helio}^1 (host) (km s ⁻¹)	Error (km s ⁻¹)	Subtraction ² ?
2012au	Ib	12:54:52.18	-10:14:50.21	2012-03-14	NGC 4790	0.13	22.9	2.8	1,344	5	Y
2012fh	IIb/Ib/c	10:43:34.05	+24:53:29.00	2012-10-18	NGC 3344	0.09	11.9	6.2	580	1	Y
2013dk	Ic	12:01:52.72	-18:52:18.30	2013-06-22	NGC 4038	0.13	21.1	3.9	1,642	12	Y
2014C	Ib	22:37:05.60	+34:24:31.90	2014-01-05	NGC 7331	0.25	13.4	2.7	816	1	Y
2014L	Ic	12:18:48.68	+14:24:43.49	2014-01-26	NGC 4254	0.11	15.2	2.0	2,407	3	Y
2014as	Ic-BL	14:00:54.49	+40:58:59.59	2014-04-18	NGC 5410	0.04	—	—	3,738	26	Y
2014cp	Ic-BL	02:25:30.46	-25:37:37.99	2014-06-23	ESO 479-G 001	0.05	45.1	7.2	4,846	3	N
2014ds	IIb	08:11:16.45	+25:10:47.39	2014-10-11	NGC 2536	0.12	—	—	4,118	17	Y
2014eh	Ic	20:25:03.86	-24:49:13.30	2014-11-03	NGC 6907	0.17	32.5	6.2	3,182	4	N
2014ei	Ib	05:03:16.39	-02:56:11.00	2014-11-05	MCG -01-13-50	0.18	57.9	3.5	4,329	4	Y
2015G	Ibn	20:37:25.58	+66:07:11.50	2015-03-23	NGC 6951	1.02	23.1	3.5	1,424	1	Y
2015K	Ic	23:35:52.26	+23:36:52.09	2015-04-25	NGC 7712	0.15	49.0	3.2	3,053	2	N
2015Q	Ib	11:47:35.081	+55:58:14.70	2015-06-17	NGC 3888	0.03	39.9	1.7	2,408	11	Y
2015U	Ibn	07:28:53.87	+33:49:10.60	2015-02-13	NGC 2388	0.16	60.9	2.3	4,134	5	Y
2015Y	Ib	09:02:37.87	+25:56:04.20	2015-04-11	NGC 2735	0.11	51.1	9.0	2,450	5	Y
2015ap	Ib	02:05:13.32	+06:06:08.39	2015-09-08	IC1776	0.12	—	—	3,410	5	Y
2016G	Ic-BL	03:03:57.74	+43:24:03.50	2016-01-09	NGC 1171	0.43	26.6	6.2	2,742	6	Y
2016P	Ic-BL	13:57:31.10	+06:05:51.00	2016-01-19	NGC 5374	0.07	68.7	10.8	4,382	7	Y
2016ajo	Ib	18:44:12.49	+24:09:29.70	2016-02-20	UGC 11344	0.34	58.5	4.2	3,836	4	Y
2016bau	Ib	11:20:59.02	+53:10:25.60	2016-03-13	NGC 3631	0.04	10.3	5.4	1,156	1	N
2016coi	Ic-BL	21:59:04.14	+18:11:10.46	2016-05-27	UGC 11868	0.23	17.2	—	1,093	5	Y
2016gcm	Ic	21:04:55.22	+65:42:29.30	2016-09-08	PGC166705	1.33	—	—	7,263	50	Y
2016gkg	IIb	01:34:14.46	-29:26:25.00	2016-09-20	NGC 613	0.05	20.9	5.7	1,481	5	N
2016gqv	Ic-pec	04:02:48.53	+01:58:15.60	2016-09-28	UGC 02936	1.23	42.8	5.1	3,813	7	Y
2016iyd	IIb	22:09:14.28	+21:31:17.51	2016-12-18	UGC 11924	0.21	—	—	3,803	5	Y
2017ein	Ic	11:52:53.25	+44:07:26.20	2017-05-25	NGC3938	0.06	12.7	7.8	809	4	N
2017iro	Ib	14:06:23.11	+50:43:20.20	2017-11-30	NGC 5480	0.05	24.2	6.0	1,856	5	Y
2018cow	Ic-BL	16:16:00.22	+22:16:04.83	2018-06-16	CGCG 137-068	0.24	—	—	4,241	39	N
2018ie	Ic-BL	10:54:01.06	-16:01:21.40	2018-01-18	NGC 3456	0.19	47.5	8.6	4,267	7	N
2019wep	Ibn	11:04:37.033	+45:58:38.95	2019-12-07	UGC 06136	0.03	—	—	7,521	11	N
2020nxt	Ibn	22:37:36.235	+35:00:07.68	2020-07-03	SDSS J223736.60+350007.4	0.21	—	—	—	—	Y
MOTJ120451.50+265946.6	Ib	12:04:51.50	+26:59:46.60	2014-10-28	NGC 4808	0.07	18.4	2.0	567	4	N
iPTF13bvn	Ib	15:00:00.152	+01:52:53.17	2013-06-16	NGC5806	0.14	24.7	3.2	1,359	5	Y

¹For the five SNe without host heliocentric velocity measurements, redshifts are adopted as follows: $z_{\text{SN} 2008\text{fi}} = 0.02600$ (Shivvers et al. 2019), $z_{\text{SN} 2008\text{fz}} = 0.133$ (Drake et al. 2010), $z_{\text{SN} 2010\text{hy}} = 0.19010$ (Shivvers et al. 2019), $z_{\text{SN} 2012\text{aa}} = 0.07990$ (Shivvers et al. 2019), and $z_{\text{SN} 2020\text{nxt}} \approx 0.02$ (Srivastav et al. 2020).

²Image subtraction is applied to remove host-galaxy contamination; see text for details.

4 RESULTS

4.1 Photometry data release

We provide our final photometry in Tables A4 (standard system) and A5 (natural system) for all 70 SESNe in our sample. On average, each SN has 81 observations (median of 58) and 22 photometric points (median of 13 points) per filter, at a cadence of 3.6 d (median of 1.2 d). SN 2016coi has the best coverage (434 points), followed by SN 2015ap (351). The total number of distinct photometric observations published in this work is 5682. Of the 70 SNe in our sample, 38 have pre-maximum coverage and thus have their peak brightness measured in at least one band. Note that although several SNe in our sample have had their photometry previously published in individual papers, the magnitudes presented herein supersede these earlier measurements because (i) for some fields requiring image subtraction we have obtained new, higher-quality templates, and (ii) better calibration sources are now available that were not used previously. Moreover, our processing is now significantly more systematic and self-consistent owing to our use of the battle-tested LOSSPhotPipeline (Stahl et al. 2019; de Jaeger et al. 2019; Stahl et al. 2020).

Note that in this release, we do not include the systematic uncertainty of 0.03 mag in *BVRI* that was determined and discussed in detail by Stahl et al. (2019). This amount of systematic uncertainty was estimated by investigating many factors that may contribute to the error, including evolution of colour terms, evolution of atmospheric terms, configurations between different telescopes, and galaxy-subtraction procedures. None of these factors contributed uncertainty over 0.03 mag, consistent with the estimate of Ganeshalingam et al. (2010). Though not included in our photometry tables (Table A4 and A5) or light-curve figures (e.g., Figure 2 and Figure A1), this uncertainty must be accounted for when combining our dataset with others. Alongside the recent LOSS photometry release for SNe Ia (Stahl et al. 2019) and SNe II (de Jaeger et al. 2019), we aim for our SESN photometry to be used and further analysed by the astronomical community.

4.2 Light curves

Figure 2 shows the apparent-magnitude light curves of all SESNe from our sample in the standard Landolt system without any extinction corrections applied. Note that we also include *Clear*-band light curves where available. Although unfiltered and thus nonstandard, it is most similar to the *R* band (Li et al. 2003). The temporal axes are all in the observer frame and shifted such that times are measured relative to the times of maximum *V*-band brightness as determined by fitting the near-maximum data with low-order Legendre polynomials. In the 37 cases where no maximum could be found via this method, the temporal axes are shifted relative to the time of the first observation. Such fitting was also applied to other bands if the data — after being supplemented with corresponding observations from Drout et al. (2011), Bianco et al. (2014), or Stritzinger et al. (2018a) — had sufficient near-maximum coverage.

4.3 Colour evolution and host extinction

Figure 3 shows the (*B* − *V*) (top left) and (*V* − *R*) (top right) colour evolution of the SESNe in our sample which have the requisite observations in both bands, after correcting for Milky Way (MW) Galactic extinction (Schlafly & Finkbeiner 2011) but not host-galaxy extinction. Individually, we find that the colours trend blue at very early

times (e.g., ∼10 d before *V*-band peak), and then become progressively more red until ∼20 d after *V*-band maximum. As a whole, however, the colours we observe span a wide range at nearly every epoch, in part because we have not (yet) performed any corrections for host extinction. As SESNe often reside in dusty star-forming regions (e.g., van Dyk et al. 1996; Kelly et al. 2008), it is likely that the extinction due to the galactic hosts of our SNe is generally the dominant component of the total line-of-sight extinction.

One useful way to estimate host extinction is to exploit its relationship with the equivalent width of Na I D absorption as measured from high-resolution spectra (e.g., Poznanski et al. 2012; Stritzinger et al. 2018b). Unfortunately, such data are difficult to obtain, and low-resolution spectra, though easier to procure, are usually not of sufficient quality for such measurements (Poznanski et al. 2011).

Distinct from spectral proxies using Na I D absorption, Drout et al. (2011) found that the (*V* − *R*) colour evolution of SESNe has a small dispersion at ∼10 d after *V*-band peak, and thus can be exploited as a useful diagnostic for estimating host-galaxy extinction (Drout et al. 2011; Taddia et al. 2015; Stritzinger et al. 2018b). We therefore follow the approach of Drout et al. (2011) to estimate the extinction induced by the host galaxies of the SNe in our sample. To do this, we measure the (*V* − *R*) colour at 10 d after *V*-band maximum, and apply extra extinction (assumed to be from the host) so that the (*V* − *R*) colour reaches 0.26 mag — the mean (*V* − *R*) colour found by Drout et al. (2011) after all corrections. We successfully applied this method to 31 SESNe in our sample with available data in both *V* and *R* at 10 d after *V*-band maximum. We note that a few SESNe in our measured sample have negative implied host-extinction values by doing this, but such values are sufficiently small to be consistent with no host extinction.

Figure 4 shows a histogram of the estimated $E(B - V)$ values for the 31 SESNe in our sample (also listed in Tab. 2) assuming a Cardelli et al. (1989) reddening law with $R_V = 3.1$. It clearly shows that SESNe usually suffer moderately-high extinction from their host galaxies, with a mean $E(B - V)$ value of 0.32 mag and standard deviation of 0.19 mag — consistent with the value found by other works using different SESN samples (Drout et al. 2011; Taddia et al. 2015; Stritzinger et al. 2018b). This mean host extinction is higher than recently studied samples of SNe Ia with mean $E(B - V) \approx 0.11$ mag (Burns et al. 2011; Stahl et al. 2019) and SNe II with mean $A_V \approx 0.9$ mag ($E(B - V) \approx 0.29$; Smartt et al. 2009).

After correcting for host extinction as described above, we plot the extinction-corrected (*B* − *V*) (bottom left) and (*V* − *R*) (bottom right) colour curves in Figure 3. The scatter in (*V* − *R*) colours is significantly decreased at 10 d after *V*-band maximum, consistent with the results of Drout et al. (2011), Taddia et al. (2015), and Stritzinger et al. (2018b). However, although its scatter is modestly reduced, the (*B* − *V*) colour curve is by no means “tight” like we observe for (*V* − *R*). This is not surprising because the host extinction is estimated from the (*V* − *R*) colour, not the (*B* − *V*) colour as proposed by Drout et al. (2011). This indicates that the (*B* − *V*) colour may not be as good a proxy as the (*V* − *R*) colour, or that the host extinction is more complicated, e.g., the hosts of SESNe are known to be with a range of R_V (e.g., Stritzinger et al. 2018b), while adopting a constant $R_V = 3.1$ to derive $E(V - R)$ would lead to errors in $E(B - V)$ and more scatter. In either case, a better method for estimating the host-galaxy extinction for SESNe would be a valuable contribution to the field.

4.4 Absolute light curve and peak magnitude

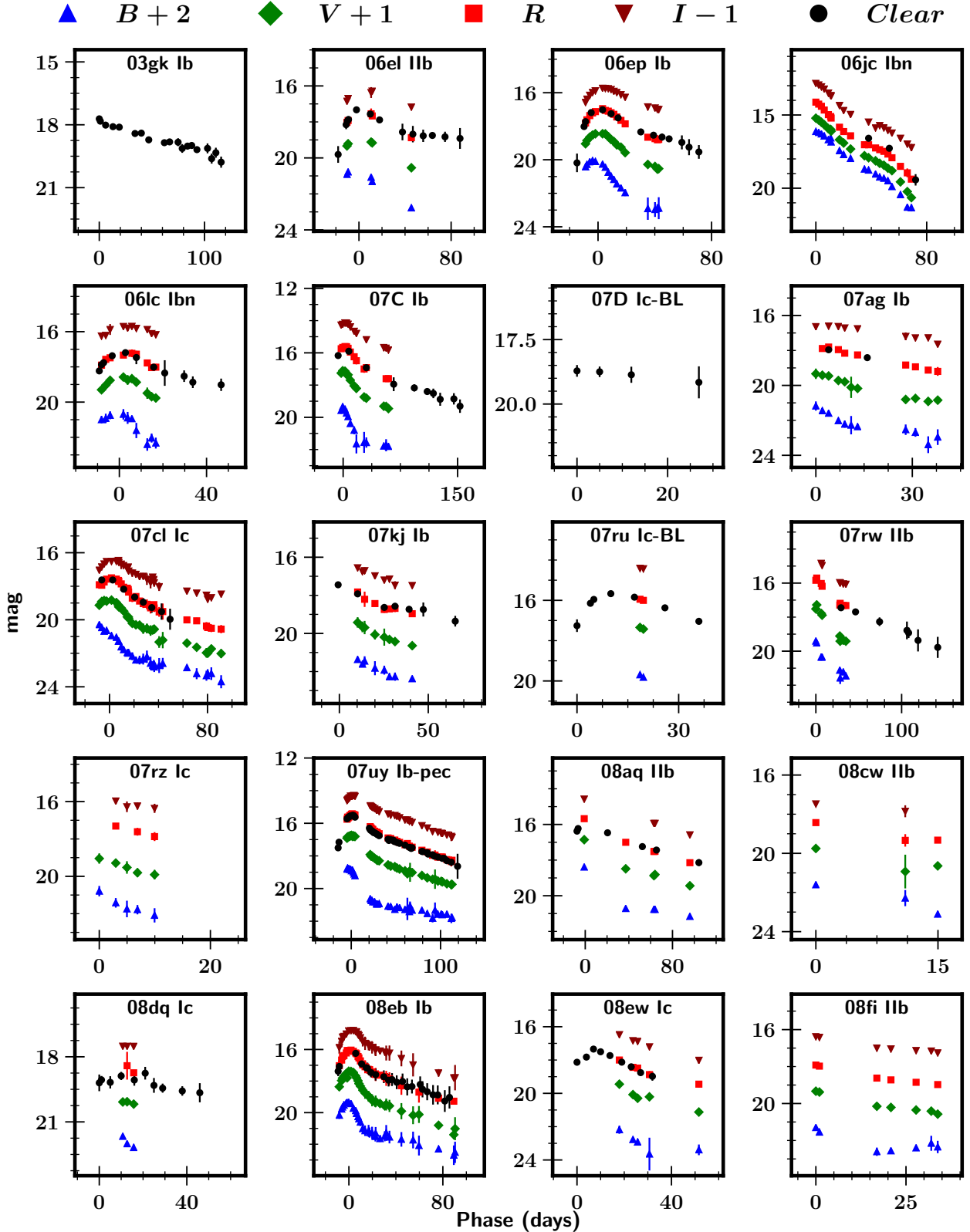


Figure 2. Apparent-magnitude light curves of the SESNe in our sample in the standard system (except for SN 2016P, which has data only in the natural system as shown in Fig. A1), without any corrections for extinction. Blue triangles are magnitudes in B , green diamonds are V , red squares are R , black circles are $Clear$, and dark-red inverted triangles are I . All dates have been shifted relative to the time of maximum V -band brightness if determined, and relative to the time of the first epoch otherwise. In each panel, the IAU name and the type are given.

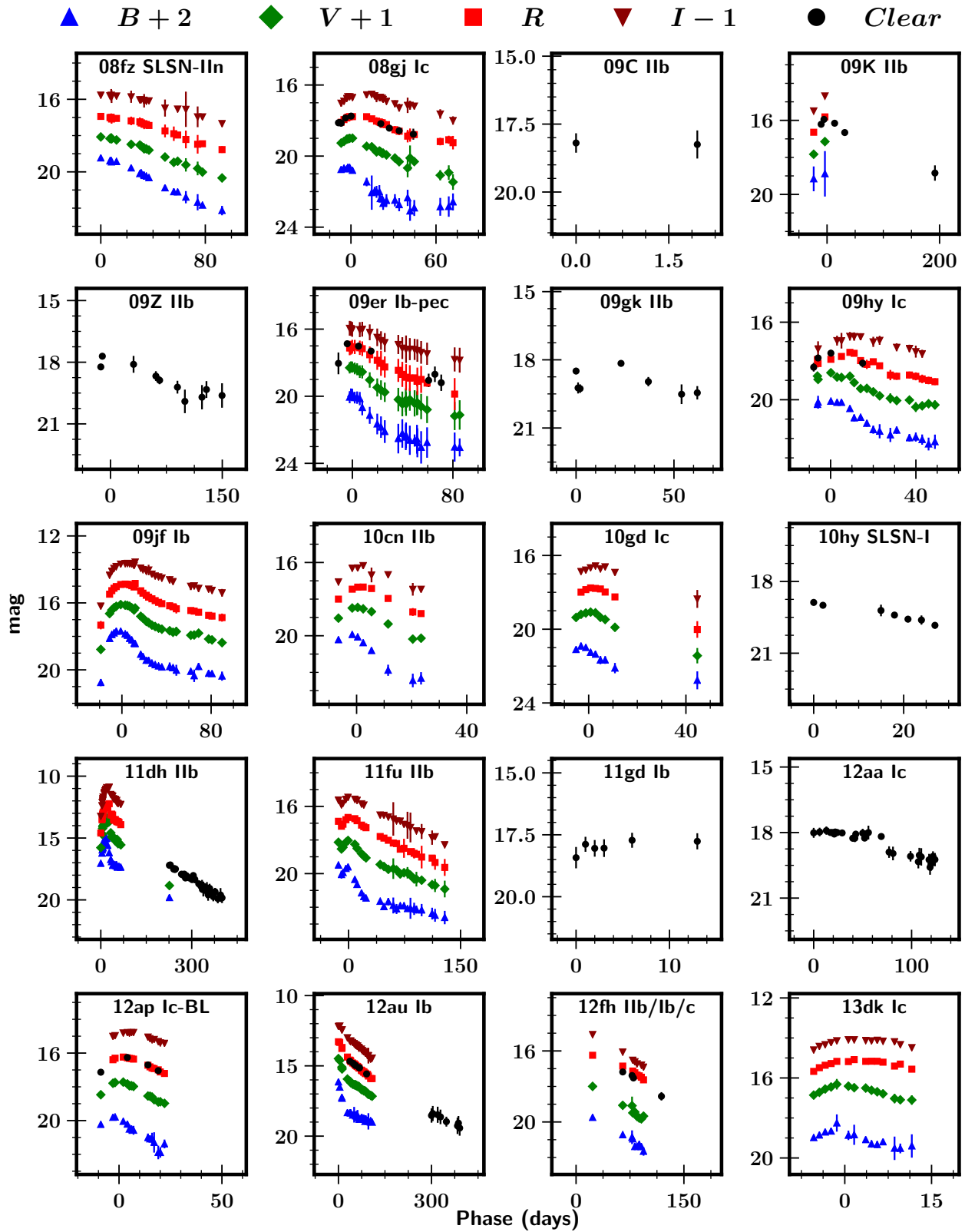


Figure 2. Continued.

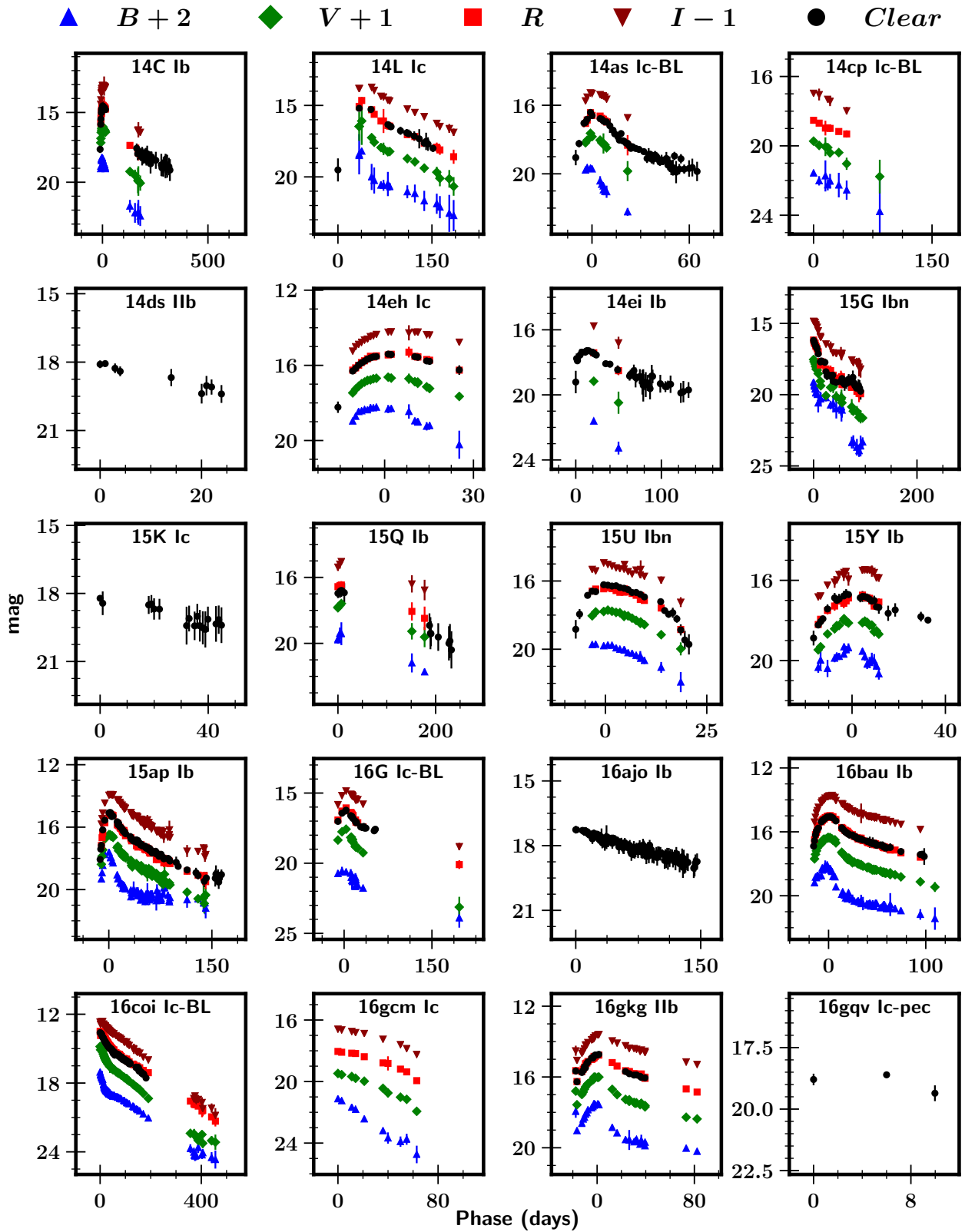
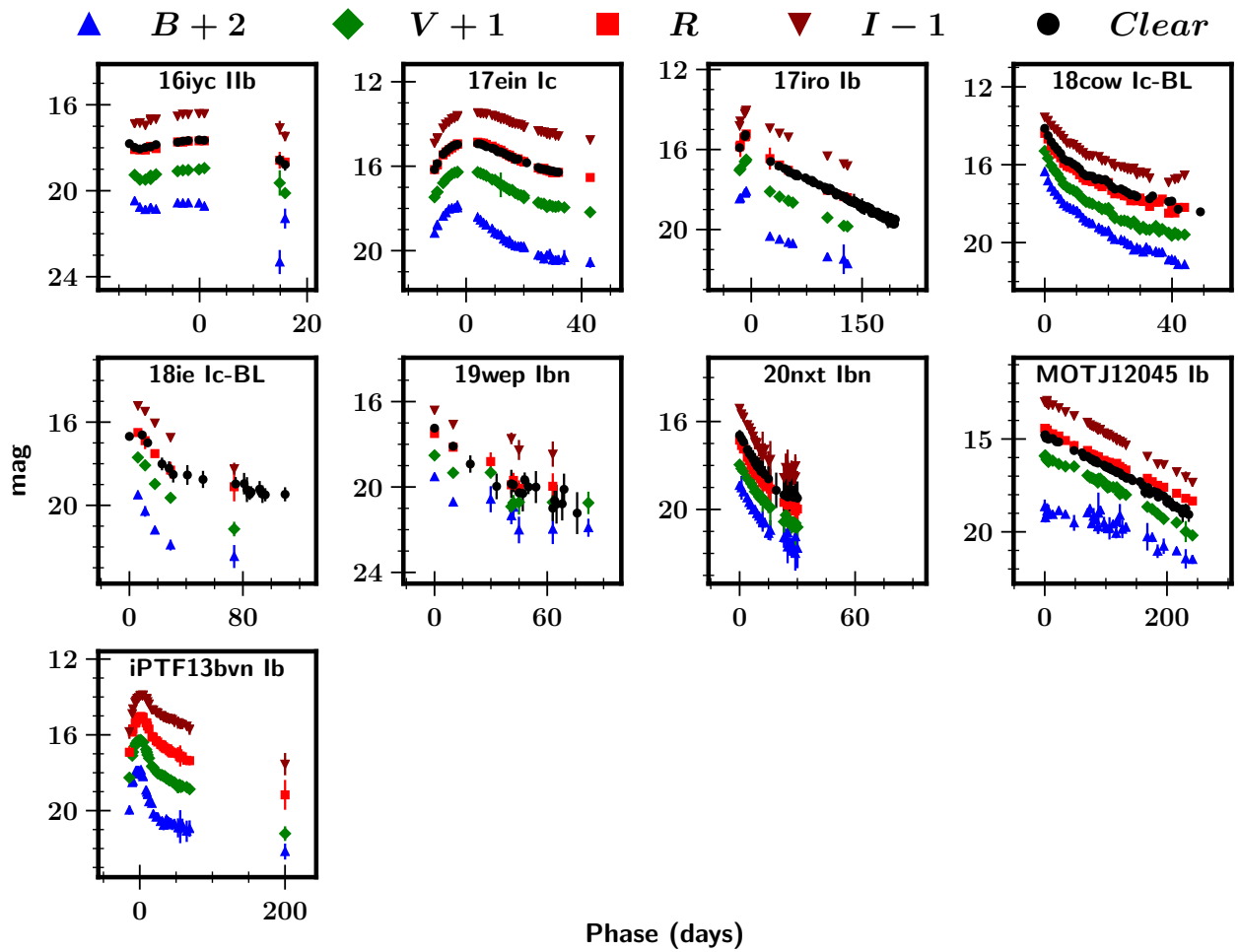


Figure 2. Continued.



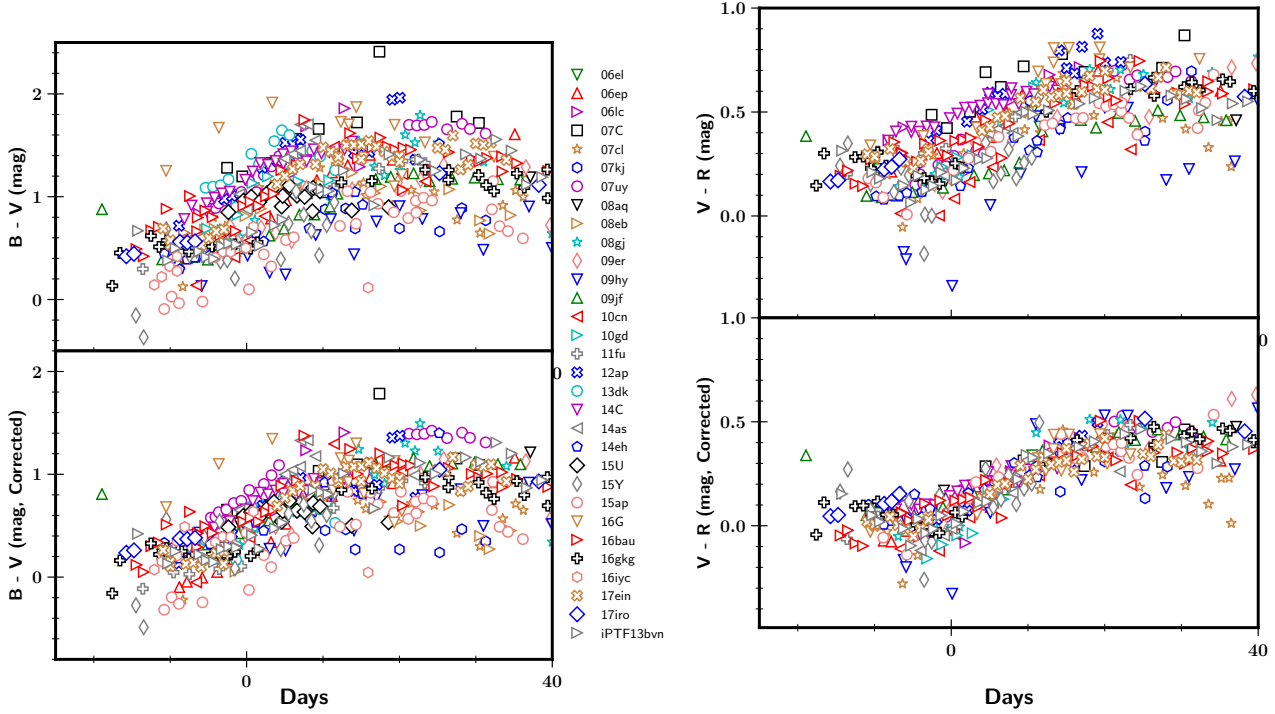


Figure 3. Left: $(B - V)$ colour evolution of the SESNe in our sample having simultaneous observations in both bands, after correction for Galactic extinction (top), and with further correction for host extinction (bottom) using the empirical colour method (see text for more details). Right: similar to the left panel, but for the $(V - R)$ colour.

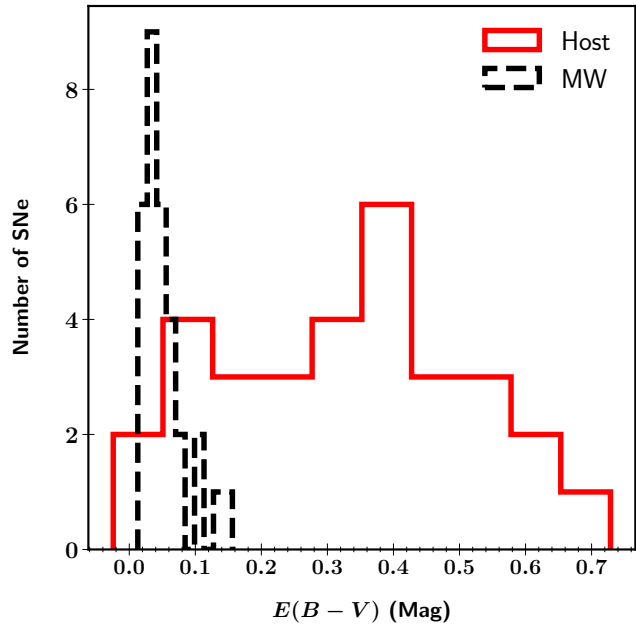


Figure 4. Distribution of host-galaxy extinction values for the 31 SESNe in our sample (solid red), revealing a mean $E(B - V)$ value of 0.32 mag with a standard deviation of 0.19 mag. The corresponding MW extinction is shown in dashed black.

Table 2. Light-Curve Properties

SN	Type	z	$E(B-V)_{\text{host}}$	$M_{\max}(R)$	$m_{\max}(U)$	$m_{\max}(B)$	$m_{\max}(g)$	$m_{\max}(V)$	$m_{\max}(R)$	$m_{\max}(r)$	$m_{\max}(\text{clear})$	$m_{\max}(I)$	$m_{\max}(i)$
2006el	IIb	0.017062	0.25	-17.88	—	18.28	—	17.60	17.33	—	—	—	17.44
2006ep	Ib	0.015134	0.45	-17.73	18.57	17.97	17.65	17.39	16.98	17.19	—	16.72	17.05
2006lc	Ibn	0.016228	0.45	-18.26	19.79	18.51	18.09	17.67	17.23	17.32	—	16.71	17.22
2007C	Ib	0.005604	0.62	-17.82	—	17.28	—	16.13	15.58	15.76	—	15.13	15.50
2007cl	Ic	0.022182	0.35	-18.27	—	—	—	17.85	17.60	17.48	—	17.42	17.69
2007kj	Ib	0.017899	0.42	—	18.30	17.92	17.74	17.66	—	17.56	—	—	17.62
2007ru	Ic-BL	0.015464	—	—	—	—	—	—	—	—	15.63	—	—
2007uy	Ib-pec	0.006494	0.30	-17.62	—	16.72	—	15.76	15.46	15.57	—	15.30	15.63
2008aq	IIb	0.007972	-0.02	—	—	16.40	—	15.84	—	—	—	—	15.95
2008eb	Ib	0.007612	0.37	-17.89	—	17.36	—	16.39	16.03	—	—	15.76	—
2008ew	Ic	0.020114	—	—	—	—	—	—	—	—	17.51	—	—
2008gj	Ic	0.023833	0.30	-17.94	—	18.64	—	18.01	17.71	—	—	17.47	—
2009K	IIb	0.011715	—	—	17.46	16.64	16.36	16.08	—	15.83	—	—	—
2009Z	IIb	0.025131	—	—	18.36	17.75	17.48	17.25	—	17.16	—	—	17.16
2009er	Ib-pec	0.034998	0.16	-19.38	—	17.92	—	17.24	17.05	17.17	—	—	17.25
2009gk	IIb	0.026505	—	—	—	—	—	—	—	—	18.05	—	—
2009hy	Ic	0.025231	-0.01	-17.63	—	18.02	—	17.68	17.66	—	—	17.77	—
2009jf	Ib	0.007942	0.07	-17.81	—	15.66	—	15.07	14.86	14.99	—	14.63	15.00
2010cn	IIb	0.026001	0.19	-18.51	—	17.90	—	17.46	17.33	—	—	17.19	—
2010gd	Ic	0.023493	0.50	-18.75	—	18.91	—	18.09	17.76	—	—	17.62	—
2011fu	IIb	0.018489	0.41	-19.02	—	17.66	—	17.06	16.67	—	—	16.49	—
2012ap	Ic-BL	0.012115	0.59	-18.29	—	17.79	—	16.71	16.23	—	—	15.78	—
2013dk	Ic	0.005477	0.73	-18.38	—	16.65	—	15.37	15.12	—	—	15.07	—
2014C	Ib	0.002722	0.50	-17.55	—	16.25	—	15.05	14.52	—	14.57	14.07	—
2014L	Ic	0.008029	—	—	—	—	—	—	—	—	—	—	—
2014as	Ic-BL	0.012469	0.37	-18.09	—	17.63	—	16.78	16.51	—	16.47	16.26	—
2014eh	Ic	0.010614	0.11	-17.57	—	16.23	—	15.63	15.40	—	15.41	15.17	—
2014ei	Ib	0.014440	—	—	—	—	—	—	—	—	17.30	—	—
2015U	Ibn	0.013790	0.36	-18.51	—	17.73	—	16.74	16.43	—	16.23	16.01	—
2015Y	Ib	0.008172	0.12	-17.14	—	17.27	—	16.84	16.78	—	16.66	16.41	—
2015ap	Ib	0.011375	0.22	-18.92	—	15.53	—	15.45	15.18	—	15.09	14.89	—
2016G	Ic-BL	0.009146	0.57	-17.79	—	18.58	—	16.56	16.07	—	16.26	15.86	—
2016bau	Ib	0.003856	0.37	-15.99	—	16.20	—	15.36	15.02	—	15.05	14.75	—
2016gkg	IIb	0.004940	0.29	-17.56	—	15.58	—	14.99	14.79	—	14.78	14.68	—
2016iyC	IIb	0.012685	0.07	-16.36	—	18.55	—	17.99	17.68	—	17.65	17.41	—
2017ein	Ic	0.002699	0.43	-16.79	—	15.91	—	15.19	14.82	—	14.87	14.45	—
2017iro	Ib	0.006191	0.18	-17.54	—	16.07	—	15.39	14.87	—	14.98	14.79	—
iPTF13bvn	Ib	0.004533	0.25	-17.65	—	15.86	—	15.26	15.03	—	—	14.90	—

Figure 5 illustrates the absolute R -band light curves of the 31 SESNe in our sample for which we are able to fully correct for extinction (i.e., correct for both MW and host-galaxy effects). Overall, the SESNe show smooth light-curve shapes with $\sim 10\text{--}20$ d rise times before maximum brightness (see Sec. 4.5 for more details), followed by a slow decay. A few Type IIb SESNe (e.g., SNe 2011fu, 2016iyc, 2016gkg) exhibit a decline dip at very early times (~ 15 d before maximum) before rising. The early-time dips for these SNe IIb can be attributed to the shock-breakout cooling tail.

The peak R -band absolute magnitude of SESNe spans a wide range from -16 mag to over -19 mag. In order to compare the peak magnitudes between different subgroups, we plot the cumulative distribution of R -band absolute magnitude (after extinction correction) in Figure 6. We find that our whole sample (29 SNe with both R peak and host-extinction measurements) has an average mean peak R absolute magnitude of -17.9 ± 0.7 mag. We also calculate the mean peak brightness for each subgroup and find a value for SNe Ib of -17.6 ± 0.7 mag (ten SNe), -17.9 ± 0.6 mag for seven SNe Ic, and -17.9 ± 1.0 mag for five SNe IIb. With admittedly small samples of three SNe Ic-BL and two SNe Ibn, we found -18.1 ± 0.3 mag and -18.4 ± 0.2 mag, respectively — brighter than the other subgroups (SNe Ib, Ic, IIb) and consistent with the conclusion reported by Taddia et al. (2015) that SNe Ic-BL are more luminous than both SNe Ib and SNe Ic, and that SNe Ic appear slightly brighter than SNe Ib. Our reported mean magnitudes are consistent with the results from Drout et al. (2011), who found -17.9 ± 0.9 mag for SNe Ib and -18.5 ± 0.8 mag for SNe Ic in the R band. Taddia et al. (2018) also reported similar trends, but in the r band, with -17.22 ± 0.60 mag, -17.66 ± 0.21 mag, and -17.45 ± 0.54 for SNe Ib, Ic, and IIb, respectively (see their Table 5).

4.5 First-light time and rise time

With progressively more SESNe discovered and observed at very early phases, it has become possible to measure the true first-light time by fitting the observed light curve. Overall, the light-curve shape of SESNe resembles that of SNe Ia. Several empirical functions have been proposed to fit SESN light curves. For example, Taddia et al. (2015) used a phenomenological model — which was first employed by Bazin et al. (2011) for fitting SNe Ia — to fit their SESN light curves. Taddia et al. (2018) also proposed a three-component function that has proven to work well. Motivated by the former, we adopt a function proposed by Zheng & Filippenko (2017) for SN Ia light-curve fitting (Zheng et al. 2017) to fit the SESN light curves in our sample. The function is given as

$$L = A' \left(\frac{t - t_0}{t_b} \right)^{\alpha_r} \left[1 + \left(\frac{t - t_0}{t_b} \right)^{s(\alpha_d)} \right]^{-2/s}, \quad (1)$$

where A' is a scaling constant, t_0 is the first-light time, t_b is the break time, α_r and α_d are the two power-law indices before and after the break, and s is a smoothing parameter. We have found that this function can provide satisfactory fits to the SESN light curves in our sample. Figure 7 presents an example of this function fit to the well-observed SN Ib iPTF13bvn. This method directly takes the first-light time t_0 as a parameter in the fitting. Following the same procedure as Zheng et al. (2017), we fit for each filter with good-quality data. We finally adopt the mean value of the first-light time from the fitting if there are more than two measurements in different filters.

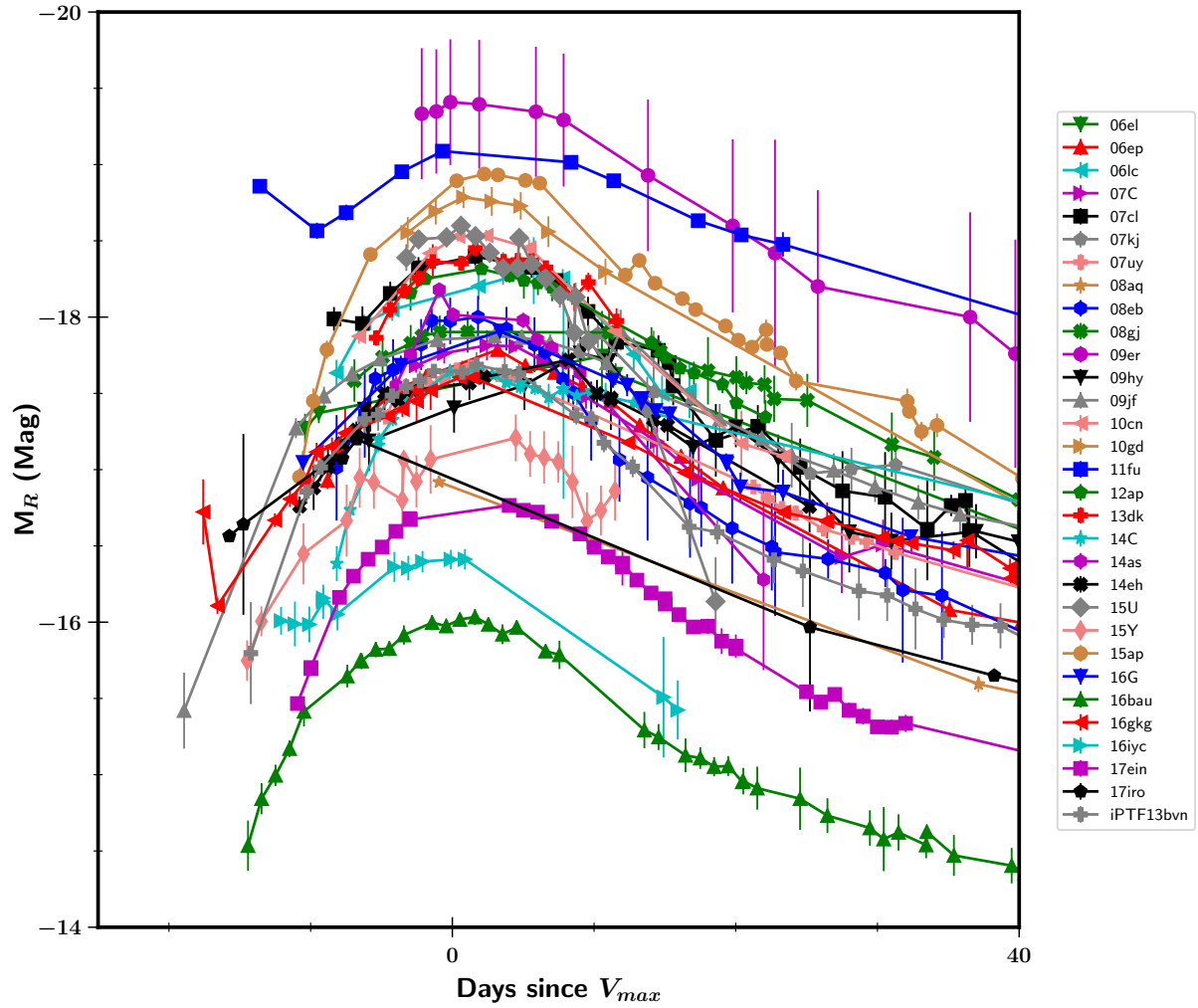


Figure 5. Absolute R -band light curves of the 31 SESNe in our sample that can be fully extinction corrected, only photometric error, not distance or host-extinction error, was included in this plot. SESNe show smooth light-curve shapes, with $\sim 10\text{--}20$ d rise times, followed by a slow post-maximum decay. A few Type IIb SESNe show a decline dip at very early times, which can be attributed to the shock-breakout cooling tail.

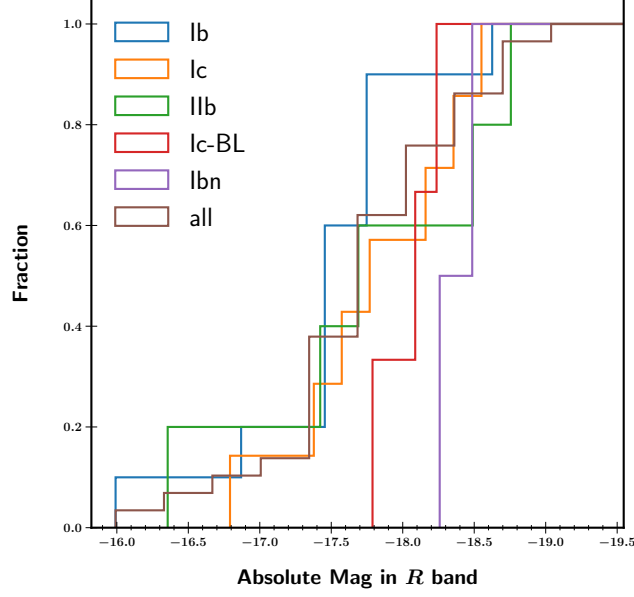


Figure 6. Cumulative distribution of the absolute R -band peak magnitudes of the 31 SESNe in our extinction-corrected sample. SESNe show a wide range from -16 mag to brighter than -19 mag. SNe Ic-BL and SNe Ibn appear on average to be more luminous than both SNe Ib and SNe Ic, and SNe Ic seem to be slightly brighter than SNe Ib.

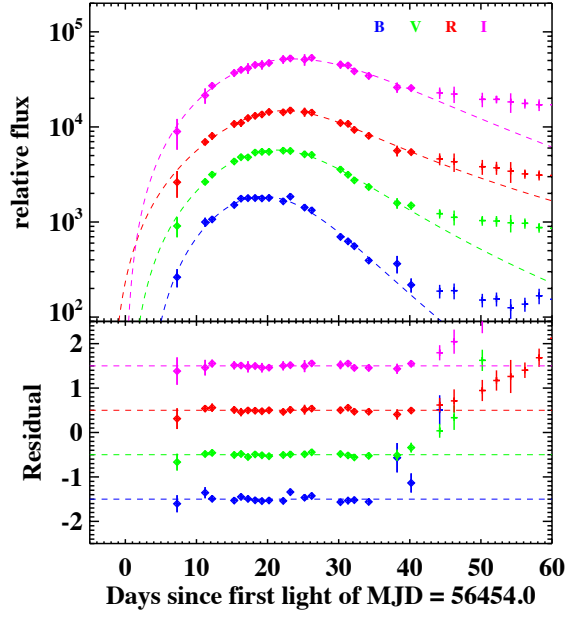


Figure 7. An example of multiband light-curve fitting to the well-observed SN iPTF13bvn using the function (see text) proposed by Zheng & Filippenko (2017), which was originally used for fitting SN Ia light curves. “Diamond” data points are included in the fitting while “cross” data points are not. This example demonstrates that the same function can also be used for fitting SESN light curves.

Table 3. Rise-time information

SN	Type	z	t_0 (MJD)	$t_r(u)$	$t_r(B)$	$t_r(g)$	$t_r(V)$	$t_r(R)$	$t_r(r)$	$t_r(Clear)$	$t_r(I)$	$t_r(i)$	$t_r(Y)$	$t_r(J)$	$t_r(H)$	$t_r(K)$
2006el	IIb	0.017062	53,958.0±1.2	—	24.5±3.8	—	25.0±2.5	25.0±5.6	—	—	—	28.5±1.5	—	—	—	—
2006ep	Ib	0.015134	53,964.7±2.4	17.7±3.0	19.8±2.4	20.4±3.0	22.2±2.6	24.3±3.0	24.0±2.8	—	25.8±2.5	25.8±2.4	28.7±2.4	30.2±2.4	30.4±2.4	—
2006lc	Ibn	0.016228	54,022.0±0.9	17.0±3.6	18.3±2.1	18.3±3.6	19.1±2.1	21.8±1.6	20.5±2.0	—	22.7±1.1	21.4±1.1	25.2±1.6	26.2±1.6	26.4±1.6	—
2007ru	Ic-BL	0.015464	54,426.5±2.1	—	—	—	—	—	—	13.8±3.2	—	—	—	—	—	—
2007uy	Ib-pec	0.006494	54,458.0±1.0	—	19.2±1.1	—	23.0±1.1	25.3±1.1	25.5±1.1	—	26.1±1.1	26.1±1.1	—	31.9±1.0	33.1±1.0	34.2±1.0
2008eb	Ib	0.007612	54,645.4±0.9	—	17.0±1.0	—	18.0±1.1	18.7±1.1	—	—	19.7±1.1	—	—	—	—	—
2009K	IIb	0.011715	54,838.3±1.6	26.4±3.2	28.2±1.9	28.9±1.9	31.0±1.7	—	32.9±1.7	—	—	38.3±1.6	37.9±1.6	41.9±1.6	—	—
2009jf	Ib	0.007942	55,097.8±1.1	—	21.0±1.5	—	23.3±1.3	25.3±1.8	25.5±1.5	—	26.5±1.3	26.8±1.8	—	31.1±1.1	32.3±1.1	35.0±1.1
iPTF13bvn	Ib	0.004533	56,454.0±1.4	—	19.5±1.5	—	21.4±1.6	22.8±1.5	—	—	24.0±1.6	—	—	—	—	—
2014C	Ib	0.002722	56,656.6±0.8	—	11.1±0.9	—	13.7±0.9	14.8±0.9	—	14.4±1.4	15.9±0.9	—	—	—	—	—
2014as	Ic-BL	0.012469	56,758.9±1.1	—	10.5±1.3	—	12.3±1.2	13.3±2.1	—	13.1±2.1	13.5±2.1	—	—	—	—	—
2014eh	Ic	0.010614	56,955.1±1.0	—	16.9±1.7	—	19.6±1.7	21.9±2.3	—	22.0±2.9	24.4±2.3	—	—	—	—	—
2014ei	Ib	0.014440	56,960.5±2.3	—	—	—	—	—	—	17.9±2.4	—	—	—	—	—	—
2015U	Ibn	0.013790	57,061.0±0.9	—	7.6±1.1	—	9.5±1.0	9.7±1.0	—	9.9±1.0	9.8±1.0	—	—	—	—	—
2015Y	Ib	0.008172	57,113.6±2.2	—	23.3±3.0	—	23.9±3.0	25.5±3.0	—	23.9±2.8	26.6±3.0	—	—	—	—	—
2015ap	Ib	0.011375	57,270.1±0.9	—	12.2±2.4	—	14.9±2.4	16.6±1.1	—	15.3±1.0	18.0±1.0	—	—	—	—	—
2016bau	Ib	0.003856	57,452.4±1.0	—	22.1±1.2	—	25.3±1.1	25.5±1.1	—	25.7±1.1	27.0±1.1	—	—	—	—	—
2016gkg	IIb	0.004940	57,644.4±0.8	—	24.9±1.1	—	26.4±1.1	27.3±0.9	—	28.1±4.0	28.3±4.0	—	—	—	—	—
2017ein	Ic	0.002699	57,895.7±0.8	—	14.8±2.6	—	17.5±2.6	19.0±2.6	—	18.1±2.6	20.1±2.6	—	—	—	—	—
Literature sample.																
2004dk	Ib	0.005247	53,213.9±0.7	—	—	—	24.7±1.9	27.7±1.9	—	—	—	—	—	—	—	—
2004ex	IIb	0.017549	53,281.7±1.0	22.9±1.7	23.9±1.7	24.3±1.7	25.4±1.1	—	26.5±1.1	—	—	28.4±1.1	32.1±1.0	27.5±1.0	30.3±1.0	—
2004fe	Ic	0.017896	53,302.6±1.2	11.9±1.3	13.3±1.6	13.9±2.1	15.1±1.6	16.7±1.7	16.6±1.4	—	—	18.0±1.3	—	—	—	—
2004gv	Ib	0.019927	53,343.9±0.9	19.2±1.1	20.6±1.1	20.6±1.1	21.9±1.6	—	23.7±1.6	—	—	25.7±1.4	26.9±0.9	26.8±0.9	32.1±0.9	—
2005hg	Ib	0.021308	53,659.4±3.2	19.9±3.2	21.5±3.2	—	23.1±3.2	25.0±3.4	25.1±3.2	—	—	27.3±3.2	—	32.3±3.2	33.6±3.2	35.8±3.2
2006T	IIb	0.008092	53,762.7±1.1	15.5±1.5	16.3±1.2	16.6±1.5	17.7±1.3	—	18.5±1.3	—	—	19.8±1.3	20.7±1.1	21.6±1.1	23.8±2.0	—
2007Y	Ib	0.004637	54,142.4±2.0	18.9±2.1	19.9±2.1	20.5±2.1	21.9±2.1	—	23.3±2.1	—	—	24.1±2.3	23.3±2.0	25.2±2.0	24.5±2.3	—
2008D	Ib	0.006494	54,468.9±0.9	—	22.2±3.7	—	23.9±3.3	—	24.7±3.7	—	—	25.5±1.0	—	—	—	—
2009bb	Ic	0.009877	54,909.6±1.0	9.1±1.4	10.3±1.4	11.5±2.7	12.9±2.7	—	13.9±2.7	—	—	14.9±2.7	20.2±1.0	18.5±1.0	17.5±1.0	—
2009iz	Ib	0.014196	55,077.3±1.1	—	28.2±1.2	—	31.0±2.8	—	33.1±2.8	—	—	36.3±1.3	—	42.9±1.1	47.1±1.1	45.3±1.1

Using the estimated first-light time along with the peak time derived above (see Sec. 4.2), one can measure the rise time after correcting for the redshift. Table 3 gives the first-light time, peak time, and rise time for the SESNe in our sample. The rise times for different bands are calculated separately when different peak times are available. In addition, we collect the infrared peak time in the Y , J , H , and K_s filters for those SNe that are also presented by Bianco et al. (2014) or Taddia et al. (2018), in order to derive the rise time in infrared bands. Ten additional SESNe are added to the rise-time sample for this analysis; they are taken from the samples published by Drout et al. (2011), Bianco et al. (2014), Stritzinger et al. (2018a), and Taddia et al. (2018), and are listed at the bottom of Table 3.

Figure 8 displays the rise time as a function of the effective wavelengths for different bands using all available fitting results for our sample. This figure is similar to Figure 10 of Taddia et al. (2015) and Figure 3 of Taddia et al. (2018). However, note that Taddia et al. (2015) use the explosion time — defined as the average between the epochs of last nondetection and first detection — instead of the first-light time, and Taddia et al. (2018) use the offset of peak time in different filters relative to the r -band peak time in their Figure 10. Consequently, we claim that the first-light times and rise times presented herein are the first true measurements of such for a large sample of SESNe. Also for the first time, we measure accurate rise times of a large sample of SESNe in infrared bands. These measurements are important for understanding the explosion properties of SESNe (see Sec. 4.6).

As can be seen in Figure 8, the rise time is generally longer in red filters than it is in blue filters, confirming the similar result found by Bianco et al. (2014), Taddia et al. (2015), and Taddia et al. (2018). The rise time in infrared bands is typically a factor of ~ 1.5 longer than in blue bands (U or B). The rise times in different subtypes of SNe also show differences, which we visualise via the cumulative distribution of the rise time for each subgroup consisting of SNe Ib, Ic, and IIb in Figure 9. A Kolmogorov-Smirnov (K-S) test comparing SNe Ib and SNe Ic in the B band gives a p -value of 0.013, showing a significant difference between the two populations, and an analogous K-S test between SNe IIb and SNe Ib in the B band gives a p -value of 0.025 — also showing a significant difference between the two populations. We find that the average rise time for SNe IIb, Ib, and Ic are 23.5, 19.9, and 13.8 d (respectively) in the B band, and 26.1, 22.6, and 19.2 d (respectively) in the R band. It is obvious that for almost all bands, SNe IIb have the longest rise times, while SNe Ic have the shortest, consistent with the findings of Valenti et al. (2011), Taddia et al. (2015), and Taddia et al. (2018). We also notice that the different rise times between each SN subtype are less clear in infrared bands compared to optical bands, though we caution that the infrared sample is much smaller.

The bottom row in Figure 9 shows the difference between rise times in the selected two bands. Typically, SNe Ic take more time for redder bands to reach peak after B -band peak compared with SNe IIb, opposite to the aforementioned rise-time relations.

4.6 Light-curve fitting and modeling

To further study the physical properties of the SESNe in our sample, we model the multiband light curves using the ^{56}Ni model subject to the following assumptions: (i) the bolometric luminosities of the photospheres of the SNe are powered by ^{56}Ni cascade decay (Arnett 1982; Chatzopoulos et al. 2012; Wang et al. 2015), (ii) the spectral energy distributions of the SNe can be described by the blackbody or ultraviolet-absorbed blackbody function (see Nicholl

et al. 2017, and references therein), and (iii) the velocities of the SN photospheres are constant at early times, and the radii of the photospheres are determined by the bolometric luminosities and the temperature at the late epochs when the temperature no longer changes (see, e.g., Eqs. 8 and 9 of Nicholl et al. 2017). We do not consider the case of interactions with dense circumstellar material, which usually make the light curves flattened at late times and are more likely related to Type IIn SNe, while the light curves in our sample do not show enough evidence for such cases. The definitions, units, and prior ranges of the free parameters of the ^{56}Ni model are given in Table 4, where the prior is uniformly sampled either linearly or in log space over the range. We employ a Markov Chain Monte Carlo (MCMC) method via the `emcee` Python package (Foreman-Mackey et al. 2013) to get the best-fit parameters and 3σ confidence ranges of the fitted parameters.

The ^{56}Ni model-fitting results for all SESNe in our sample are shown in Figure A2, except SN 2009C for which there is not enough data to meaningfully constrain the fitting. The best-fitted parameter values are given in Table A1, where we also list in parentheses the median values for comparison. As one can see, for most of the SNe, though the B -band fitting deviates more than other filters for some cases, our ^{56}Ni model can fit the general observed light curves with reasonable physical parameters.

However, for a group of SNe with double peaks or rebrightening after initial fading (including SNe 2011fu, 2015Y, 2016gkg, and 2016iyc), our simple ^{56}Ni model fails to adequately fit the early-time initial decay. In these cases, we therefore adopt an additional cooling component and refit the light curve. The new cooling plus ^{56}Ni model contains three additional parameters: (i) the mass of the extended envelope (M_e), (ii) the radius of the extended envelope ($R_{e,12}$), and (iii) the energy passed into the extended envelope ($E_{e,50}$) from the SN core (Piro et al. 2021). The cooling plus ^{56}Ni model can better fit the light curves as shown in Figure A3, and the new fitting results are given in Table A2.

For another group of four SNe (including SNe 2008fz, 2010hy, 2012aa, and 2018cow), the ^{56}Ni model results suggest extremely high ^{56}Ni masses, some even higher than the ejecta mass, which is clearly unphysical. For these four luminous or superluminous SNe, we therefore adopt the magnetar model (Kasen & Bildsten 2010; Woosley 2010; Chatzopoulos et al. 2012; Wang et al. 2015; Dai et al. 2016) to refit the light curves. Three new parameters are included compared to the ^{56}Ni model (also listed in Table A1): the initial period (P_0), the magnetic field strength of the magnetar ($B_{p,14}$), and the gamma-ray opacity of magnetar photons ($\kappa_{\gamma,\text{mag}}$). The magnetar model fitting is shown in Figure A4, and the results are given in Table A3. Compared to the ^{56}Ni model, the magnetar model provides comparable fitting results for the light curves, but with more reasonable physical parameters, indicating that a small fraction of SESNe may be powered by central magnetars⁸.

To summarise, Figure 10 shows the cumulative distribution of the four parameters (M_{ej} , v_9 , M_{Ni} , and T_f) from the model fitting. We find that SNe Ic tend to have lower ejecta masses and also slower ejecta velocities, on average, compared to SNe Ib and SNe IIb. On the other hand, the ^{56}Ni mass of SNe Ic tends to be higher than in SNe Ib and SNe IIb, consistent with the findings of Prentice et al. (2016) (see Table 10 in the paper). Anderson (2019) reached a similar conclusion (see Table 1 in their paper) that SNe Ic have

⁸ Note that we cannot exclude the possibility of a hidden (fainter) magnetar in other SESNe, but those SESNe do not require the fainter magnetar in the model fitting.

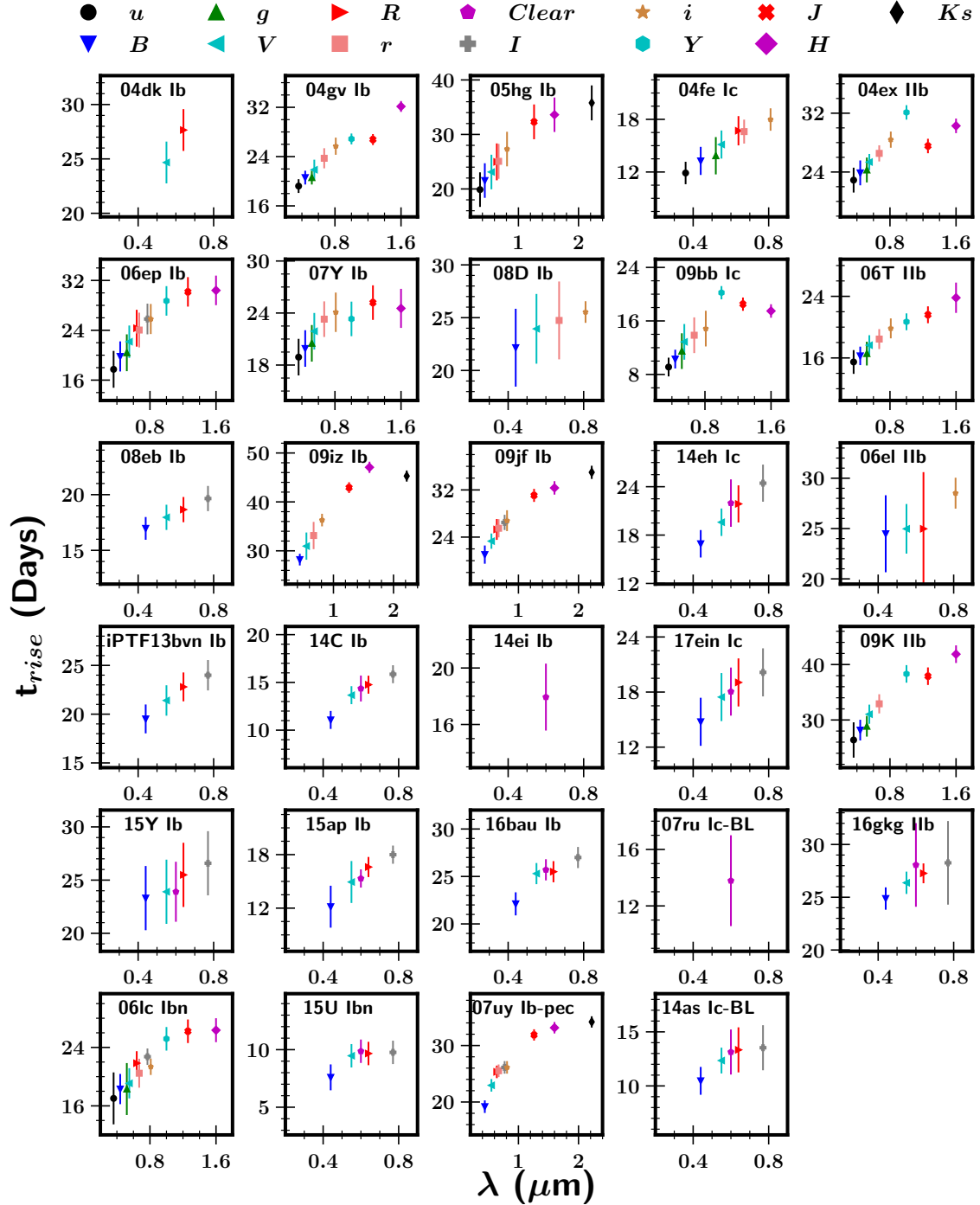


Figure 8. Rise time derived from 29 SESNe as a function of the effective wavelengths for different bands, colour coded as shown in the top legend. The rise time is generally longer in redder filters than it is in bluer filters. The rise time in infrared bands is typically a factor of ~ 1.5 longer than in blue bands (U or B).

higher ^{56}Ni mass than SNe IIb, though their estimate of the ^{56}Ni mass for SNe Ib is comparable to that of SNe Ic. The temperature floor of the photosphere distribution shows no significant difference between different subtypes.

5 CONCLUSION

In this paper, we have presented multiband ($BVRI$, along with some *Clear*) light curves of a large sample of SESNe observed by the KAIT and Nickel telescopes at Lick Observatory under the LOSS follow-up program from 2003 through 2020. Our data are processed in a homogeneous fashion, and here we publicly release all derived data products to the supernova community. Our main results are as follows.

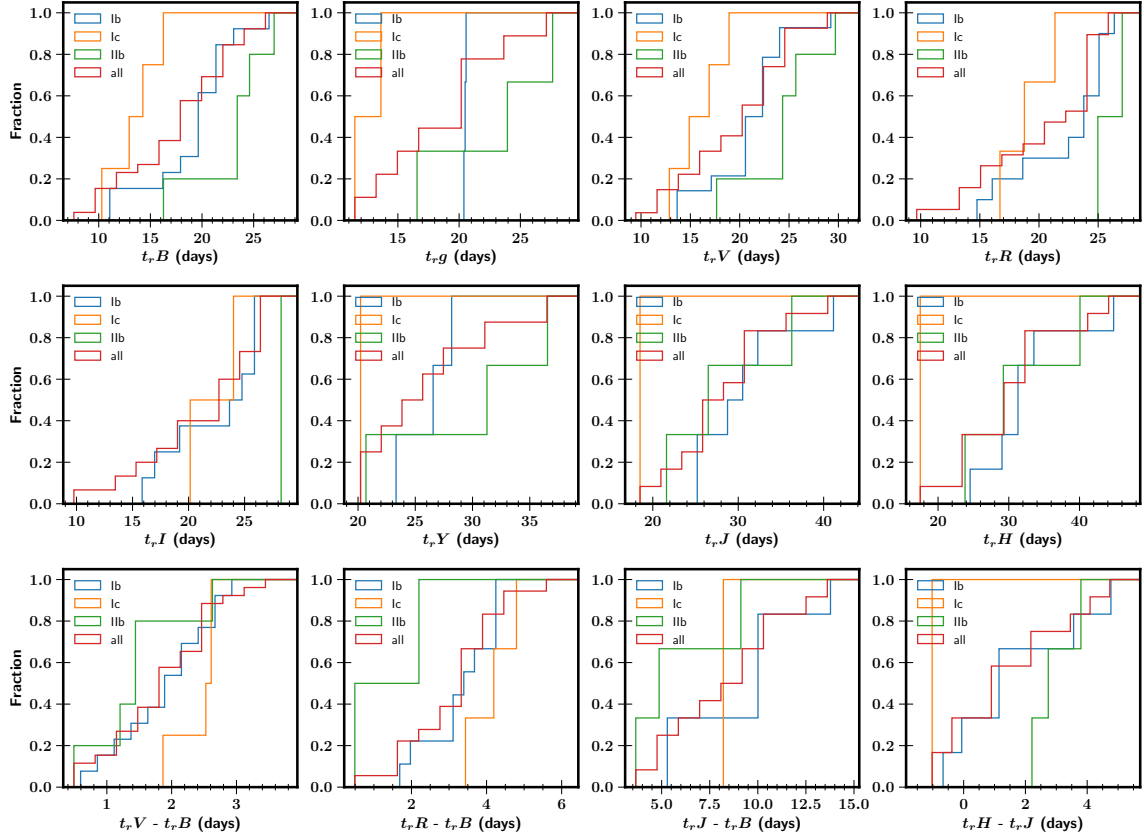


Figure 9. Top two rows: Cumulative distribution of rise time in eight different filters. K-S tests show significant differences between SNe Ib and SNe Ic, and also between SNe IIb and SNe Ib. The average rise times for SNe IIb, Ib, and Ic are 23.5, 19.9, and 13.8 d (respectively) in the B band. For almost all bands, SNe IIb have the longest rise time, while SNe Ic have the shortest rise time. Bottom row: The difference of rise time in the selected two bands. SNe Ic take more time for the redder band to reach peak after B -band peak compared to SNe IIb, opposite to the rise-time relation.

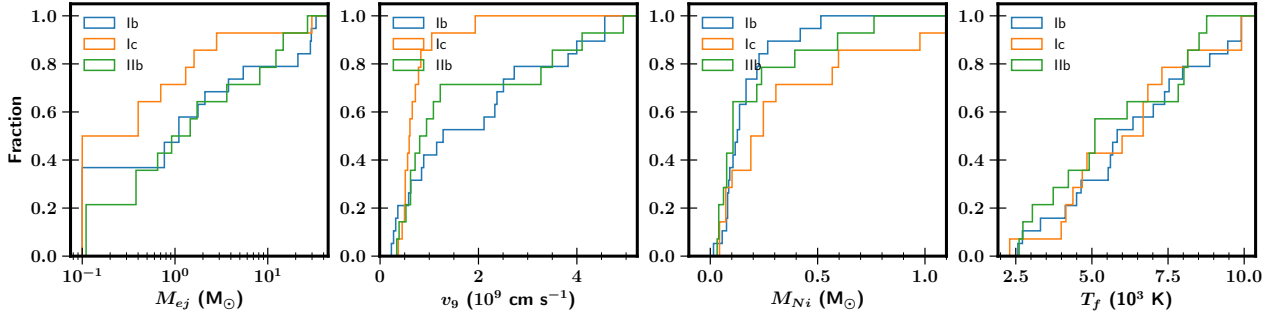


Figure 10. Cumulative distributions of the four parameters (M_{ej} , v_9 , M_{Ni} , and T_f) derived from model fitting. Compared to SNe Ib and SNe IIb, SNe Ic tend to have higher ejecta masses and also higher ejecta velocities, on average, but lower ^{56}Ni mass. The temperature floor of the photosphere distribution shows no significant difference between different subtypes.

(i) We significantly enlarge the SESNe sample by adding 70 SESNe observed by LOSS.

(ii) We confirm that SESNe usually suffer moderately high extinction from their host galaxies. Quantitatively, we find a mean $E(B - V)$ value of 0.32 mag, substantially higher than the MW extinction, and also higher than that of SN Ia and SN II samples.

(iii) The peak R -band absolute magnitude of SESNe shows a wide range from -16 mag to brighter than -19 mag. SNe Ic-BL are more luminous than both SNe Ib and SNe Ic, and SNe Ic appear to be slightly brighter than SNe Ib.

(iv) SESNe exhibit smooth light-curve shapes with a ~ 10 –20 d rising phase before reaching maximum brightness, followed by a slow decay. A few SNe IIb show a decline dip at very early times before rising again, which can be attributed to the shock-breakout cooling tail.

(v) For the first time, we derive reliable, robust measurements of the rise times for a large sample of SESNe in both optical and infrared bands. Our results show that SESNe rise faster in blue bands than in red bands.

(vi) Helium-poor SNe (SNe Ic) rise to maximum faster than

Table 4. The definitions, units, and prior ranges of the parameters of the fitting models .

Parameter	Definition	Unit	Posterior
⁵⁶ Ni model			
M_{ej}	ejecta mass	M_{\odot}	[0.1, 50]
v_9	ejecta velocity	10^9 cm s^{-1}	[0.1, 5.0(10.0)] ^a
M_{Ni}	⁵⁶ Ni mass	M_{\odot}	[0.001, 2.0(20.0)] ^a
$\kappa_{\gamma,\text{Ni}}$	gamma-ray opacity of ⁵⁶ Ni-cascade-decay photons	$\text{cm}^2 \text{ g}^{-1}$	[0.027, 10 ⁴] ^c
T_f	temperature floor of the photosphere	10^3 K	[1000, 10, 000]
t_{shift}^b	explosion time relative to the first data	days	[-20, 0]
Cooling model with three additional parameters compared to the ⁵⁶ Ni model.			
M_e	envelope mass	M_{\odot}	[0.01, 30]
$R_{e,12}$	envelope radius	10^{12} cm	[10, 3000]
$E_{e,50}$	energy passed into the envelope from SN core	$10^{50} \text{ erg s}^{-1}$	[10 ⁻⁵ , 10 ³] ^c
Magnetar model with three different parameters compared to the ⁵⁶ Ni model, but dropped M_{Ni} and $\kappa_{\gamma,\text{Ni}}$.			
P_0	initial period of the magnetar	ms	[0.8, 50]
$B_{p,14}$	magnetic field strength of the magnetar	10^{14} G	[0.1, 100]
$\kappa_{\gamma,\text{mag}}$	gamma-ray opacity of magnetar photons	$\text{cm}^2 \text{ g}^{-1}$	[0.01, 10 ⁴] ^c

^aFor four luminous or superluminous SNe (SNe 2008fz, 2010hy, 2012aa, and 2018cow; see Table A3), the upper limits of prior of v_9 and M_{Ni} are set to be 10 and 20.0, respectively.

^bFor the SNe whose explosion date (t_0) had been inferred (see Table 3), the t_{shift} parameter was set to be fixed.

^cParameter was distributed in log space.

helium-rich SNe (SNe Ib and IIb). Average rise times for SNe IIb, Ib, and Ic are 23.5, 19.9, and 13.8 d (respectively) in the *B* band, and 26.1, 22.6, and 19.2 d (respectively) in the *R* band. K-S tests show significant differences between normal SNe Ib and SNe Ic, and also between SNe IIb and SNe Ib.

(vii) SNe Ic tend to have lower ejecta masses and also slower ejecta velocities, on average, compared to SNe Ib and SNe IIb, but with higher ⁵⁶Ni mass.

ACKNOWLEDGEMENTS

We thank Jenifer Rene Gross and Alessondra Springmann for their effort in taking Lick/Nickel data. We are grateful to the staff at Lick Observatory for their assistance with the Nickel telescope and KAIT. KAIT and its ongoing operation were made possible by donations from Sun Microsystems, Inc., the Hewlett-Packard Company, Auto Scope Corporation, Lick Observatory, the National Science Foundation (NSF), the University of California, the Sylvia & Jim Katzman Foundation, and the TABASGO Foundation. Research at Lick Observatory is partially supported by a generous gift from Google.

Support for A.V.F.’s supernova group has been provided by the NSF, Marc J. Staley (whose fellowship partly funded B.E.S. whilst contributing to the work presented herein as a graduate student), the Richard and Rhoda Goldman Fund, the TABASGO Foundation, Gary and Cynthia Bengier (who provided financial support for T.deJ. via the Bengier Postdoctoral fellowship), the Christopher R. Redlich Fund, and the UC Berkeley Miller Institute for Basic Research in Science (in which A.V.F. was a Miller Senior Fellow at the time of this research). In addition, we greatly appreciate contributions from numerous individuals, including Charles Baxter and Jinee Tao, George and Sharon Bensch Greg and Patty Bernstein,

Firmin Berta, Jack Bertges, Marc and Cristina Bensadoun, Greg and Patty Bernstein, Frank and Roberta Bliss, Ann and Gordon Brown, Eliza Brown and Hal Candee, Kathy Burck and Gilbert Montoya, Alan and Jane Chew, Christopher Cook, David and Linda Cornfield, Michael Danylchuk, Robert Davenport, Jim and Hildy DeFrisco, Alli and Byron Deeter, Tim and Melissa Draper, William and Phyllis Draper, Luke Ellis and Laura Sawczuk, Jim Erbs and Shan Atkins, Alan Eustace and Kathy Kwan, Art and Cindy Folker, Peter and Robin Frazier, David Friedberg, Harvey Glasser, Charles and Gretchen Gooding, Alan Gould and Diane Tokugawa, Richard Gregor, Thomas and Dana Grogan, Timothy and Judi Hachman Michael and Virginia Halloran, Gregory Hirsch and Kathy Long, Alan and Gladys Hoefer, Jerry and Patti Hume, Charles and Patricia Hunt, Stephen and Catherine Imbler, Adam and Rita Kablanian, Heidi Gerster Kikawada, Roger and Jody Lawler, Arthur and Rita Levinson, Jesse Levinson, Kenneth and Gloria Levy, Greg Losito and Ronnie Bayduza, Walter and Karen Loewenstein, Peter Maier, DuBose and Nancy Montgomery, Rand Morimoto and Ana Henderson, Sunil Nagaraj and Mary Katherine Stimmier, Peter and Kristan Norvig, James and Marie O’Brien, Emilie and Doug Ogden, Paul and Sandra Otellini, Margaret Renn, Robina Ricciello, Leslie Roberts, Jeanne and Sanford Robertson, Paul Robinson, Eric Rudney, Sissy Sailors and Red Conger, Geraldine and David Sandor, Tom and Cathy Saxton, Stanley and Miriam Schiffman, Thomas and Alison Schneider, Ajay Shah and Lata Krishnan, Alex and Irina Shubat, Silicon Valley Community Foundation, Bruce and Debby Smith, Mary-Lou Smulders and Nicholas Hodson, Hans Spiller, Alan and Janet Stanford, Richard and Shari Stegman, Hugh Stuart Center Charitable Trust, Toby Stuart, Gerald and Virginia Weiss, Clark and Sharon Winslow, Ron and Geri Wohl, Weldon and Ruth Wood, David and Angie Yancey, Tom Zdeblick, and many others. X.G.W. is supported by the National Natural Science Foundation of

China (NSFC grant 11673006) and the Guangxi Science Foundation (grants 2016GXNSFFA380006 and 2017AD22006).

This research has made use of the NASA/IPAC Extragalactic Database (NED), which is operated by the Jet Propulsion Laboratory, California Institute of Technology, under contract with NASA. The Pan-STARRS1 Surveys (PS1) and the PS1 public science archive have been made possible through contributions by the Institute for Astronomy, the University of Hawaii, the Pan-STARRS Project Office, the Max-Planck Society and its participating institutes, the Max Planck Institute for Astronomy, Heidelberg and the Max Planck Institute for Extraterrestrial Physics, Garching, The Johns Hopkins University, Durham University, the University of Edinburgh, the Queen's University Belfast, the Harvard-Smithsonian Center for Astrophysics, the Las Cumbres Observatory Global Telescope Network Incorporated, the National Central University of Taiwan, the Space Telescope Science Institute, NASA under grant NNX08AR22G issued through the Planetary Science Division of the NASA Science Mission Directorate, the National Science Foundation grant AST-1238877, the University of Maryland, Eotvos Lorand University (ELTE), the Los Alamos National Laboratory, and the Gordon and Betty Moore Foundation. Funding for the Sloan Digital Sky Survey (SDSS) has been provided by the Alfred P. Sloan Foundation, the Participating Institutions, NASA, the NSF, the U.S. Department of Energy, the Japanese Monbukagakusho, and the Max Planck Society. The SDSS Web site is <http://www.sdss.org/>. The SDSS is managed by the Astrophysical Research Consortium (ARC) for the Participating Institutions. The Participating Institutions are The University of Chicago, Fermilab, the Institute for Advanced Study, the Japan Participation Group, The Johns Hopkins University, Los Alamos National Laboratory, the Max-Planck-Institute for Astronomy (MPIA), the Max-Planck-Institute for Astrophysics (MPA), New Mexico State University, University of Pittsburgh, Princeton University, the United States Naval Observatory, and the University of Washington.

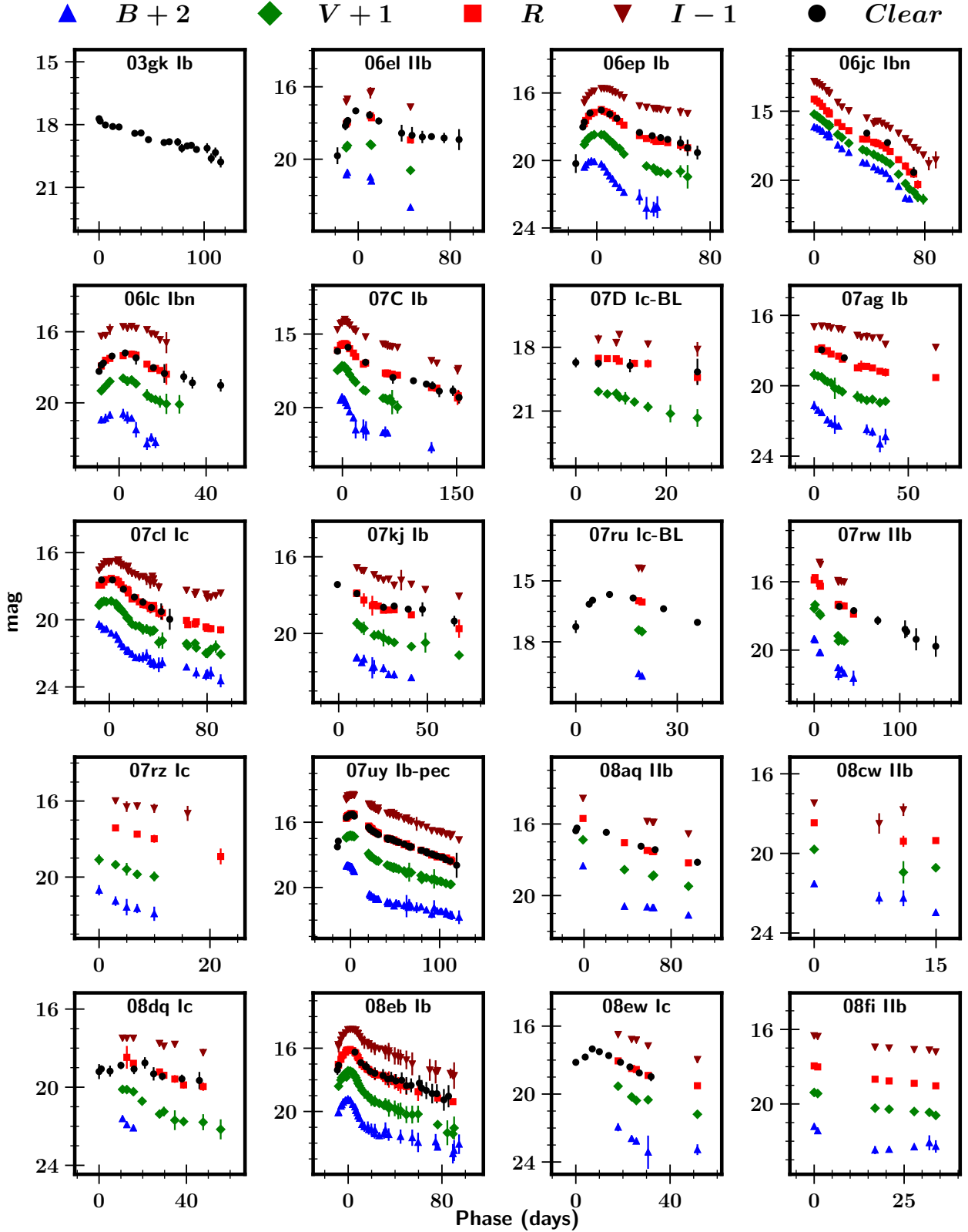
AVAILABILITY OF DATA

The data underlying this article are available in the article and in its online supplementary material.

REFERENCES

- Anderson J. P., 2019, *A&A*, **628**, A7
 Arnett W. D., 1982, *ApJ*, **253**, 785
 Bazin G., et al., 2011, *A&A*, **534**, A43
 Bianco F. B., et al., 2014, *ApJS*, **213**, 19
 Burns C. R., et al., 2011, *AJ*, **141**, 19
 Cardelli J. A., Clayton G. C., Mathis J. S., 1989, *ApJ*, **345**, 245
 Chatzopoulos E., Wheeler J. C., Vinko J., 2012, *ApJ*, **746**, 121
 Conti P. S., 1975, Memoires of the Societe Royale des Sciences de Liege, **9**, 193
 Dai Z. G., Wang S. Q., Wang J. S., Wang L. J., Yu Y. W., 2016, *ApJ*, **817**, 132
 de Jaeger T., et al., 2019, *MNRAS*, **490**, 2799
 Drake A. J., et al., 2010, *ApJ*, **718**, L127
 Drout M. R., et al., 2011, *ApJ*, **741**, 97
 Eldridge J. J., Fraser M., Smartt S. J., Maund J. R., Crockett R. M., 2013, *MNRAS*, **436**, 774
 Filippenko A. V., 1988, *AJ*, **96**, 1941
 Filippenko A. V., 1997, *ARA&A*, **35**, 309
 Filippenko A. V., Matheson T., Ho L. C., 1993, *ApJ*, **415**, L103
 Filippenko A. V., Li W. D., Treffers R. R., Modjaz M., 2001, in Paczynski B., Chen W.-P., Lemme C., eds, Astronomical Society of the Pacific Conference Series Vol. 246, IAU Colloq. 183: Small Telescope Astronomy on Global Scales. p. 121
 Foley R. J., Smith N., Ganeshalingam M., Li W., Chornock R., Filippenko A. V., 2007, *ApJ*, **657**, L105
 Foreman-Mackey D., Hogg D. W., Lang D., Goodman J., 2013, *PASP*, **125**, 306
 Fraser M., et al., 2021, arXiv e-prints, [p. arXiv:2108.07278](https://arxiv.org/abs/2108.07278)
 Gal-Yam A., 2017, Observational and Physical Classification of Supernovae. p. 195, doi:10.1007/978-3-319-21846-5_35
 Gal-Yam A., et al., 2014, *Nature*, **509**, 471
 Gal-Yam A., et al., 2021, arXiv e-prints, [p. arXiv:2111.12435](https://arxiv.org/abs/2111.12435)
 Ganeshalingam M., Li W., Filippenko A. V., et al., 2010, *ApJS*, **190**, 418
 Hosseinzadeh G., et al., 2017, *ApJ*, **836**, 158
 Kasen D., Bildsten L., 2010, *ApJ*, **717**, 245
 Kelly P. L., Kirshner R. P., Pahre M., 2008, *ApJ*, **687**, 1201
 Landolt A. U., 1983, *AJ*, **88**, 439
 Landolt A. U., 1992, *AJ*, **104**, 340
 Lang D., Hogg D. W., Mierle K., Blanton M., Roweis S., 2010, *AJ*, **139**, 1782
 Li W., Filippenko A. V., Chornock R., Jha S., 2003, *PASP*, **115**, 844
 Li W., Leaman J., Chornock R., et al., 2011, *MNRAS*, **412**, 1441
 Matheson T., 2001, *PASP*, **113**, 1155
 Modjaz M., et al., 2014, *AJ*, **147**, 99
 Nicholl M., Guillochon J., Berger E., 2017, *ApJ*, **850**, 55
 Pastorello A., et al., 2007, *Nature*, **447**, 829
 Pastorello A., et al., 2021, Transient Name Server AstroNote, **71**, 1
 Perley D. A., et al., 2021, arXiv e-prints, [p. arXiv:2111.12110](https://arxiv.org/abs/2111.12110)
 Piro A. L., Haynie A., Yao Y., 2021, *ApJ*, **909**, 209
 Podsiadlowski P., Joss P. C., Hsu J. J. L., 1992, *ApJ*, **391**, 246
 Poznanski D., Ganeshalingam M., Silverman J. M., Filippenko A. V., 2011, *MNRAS*, **415**, L81
 Poznanski D., Prochaska J. X., Bloom J. S., 2012, *MNRAS*, **426**, 1465
 Prentice S. J., et al., 2016, *MNRAS*, **458**, 2973
 Sana H., et al., 2012, *Science*, **337**, 444
 Schlafly E. F., Finkbeiner D. P., 2011, *ApJ*, **737**, 103
 Shrivvers I., et al., 2019, *MNRAS*, **482**, 1545
 Smartt S. J., Eldridge J. J., Crockett R. M., Maund J. R., 2009, *MNRAS*, **395**, 1409
 Smith N., Owocki S. P., 2006, *ApJ*, **645**, L45
 Srivastav S., Smartt S. J., McBrien O., Smith K. W., Young D. R., Gillanders J., 2020, Transient Name Server Classification Report, **2020-2148**, 1
 Stahl B. E., et al., 2019, *MNRAS*, **490**, 3882
 Stahl B. E., Martínez-Palomera J., Zheng W., de Jaeger T., Filippenko A. V., Bloom J. S., 2020, *MNRAS*, **496**, 3553
 Stetson P. B., 1987, *PASP*, **99**, 191
 Stritzinger M., Sunzeff N. B., Hamuy M., Challis P., Demarco R., Germany L., Soderberg A. M., 2005, *PASP*, **117**, 810
 Stritzinger M. D., et al., 2018a, *A&A*, **609**, A134
 Stritzinger M. D., et al., 2018b, *A&A*, **609**, A135
 Taddia F., et al., 2015, *A&A*, **574**, A60
 Taddia F., et al., 2018, *A&A*, **609**, A136
 Tonry J. L., et al., 2012, *ApJ*, **750**, 99
 Valenti S., et al., 2011, *MNRAS*, **416**, 3138
 Van Dyk S. D., Hamuy M., Filippenko A. V., 1996, *AJ*, **111**, 2017
 Wang S. Q., Wang L. J., Dai Z. G., Wu X. F., 2015, *ApJ*, **807**, 147
 Woosley S. E., 2010, *ApJ*, **719**, L204
 Woosley S. E., Bloom J. S., 2006, *ARA&A*, **44**, 507
 Zheng W., Filippenko A. V., 2017, *ApJ*, **838**, L4
 Zheng W., Kelly P. L., Filippenko A. V., 2017, *ApJ*, **848**, 66

APPENDIX A: ONLINE SUPPLEMENTARY

**Figure A1.** Same as Figure 2, but in the natural system.

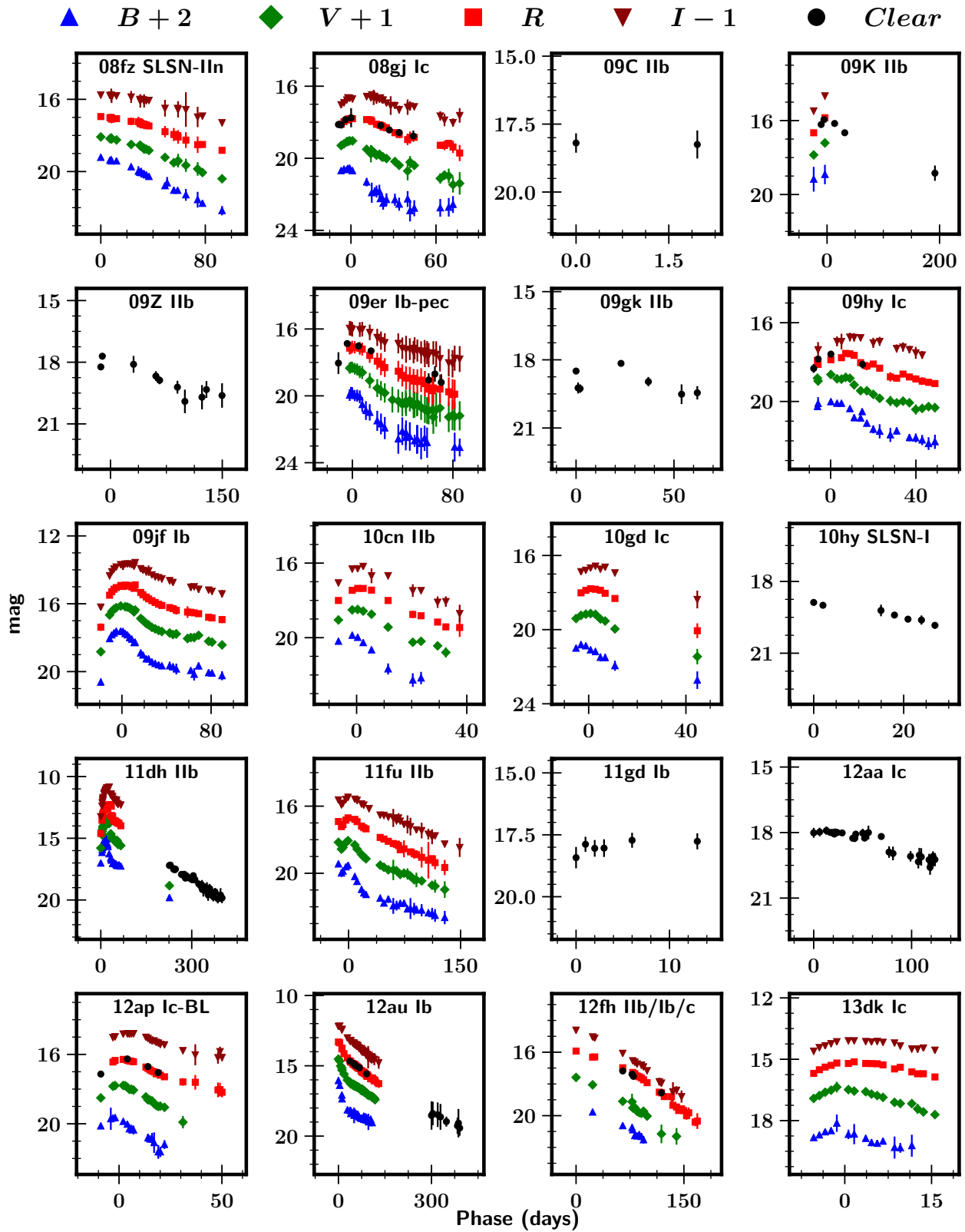


Figure A1. Continued.

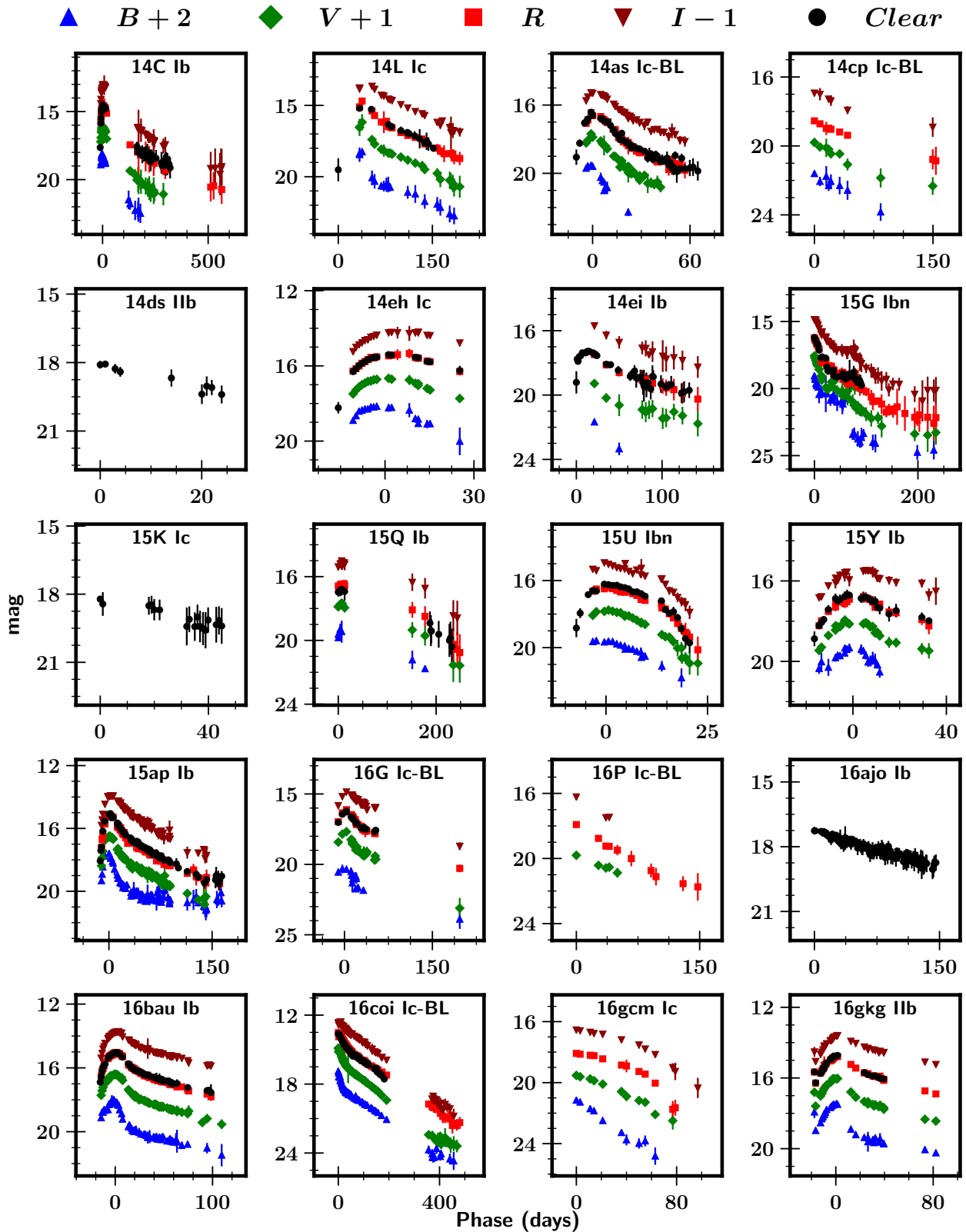


Figure A1. Continued.

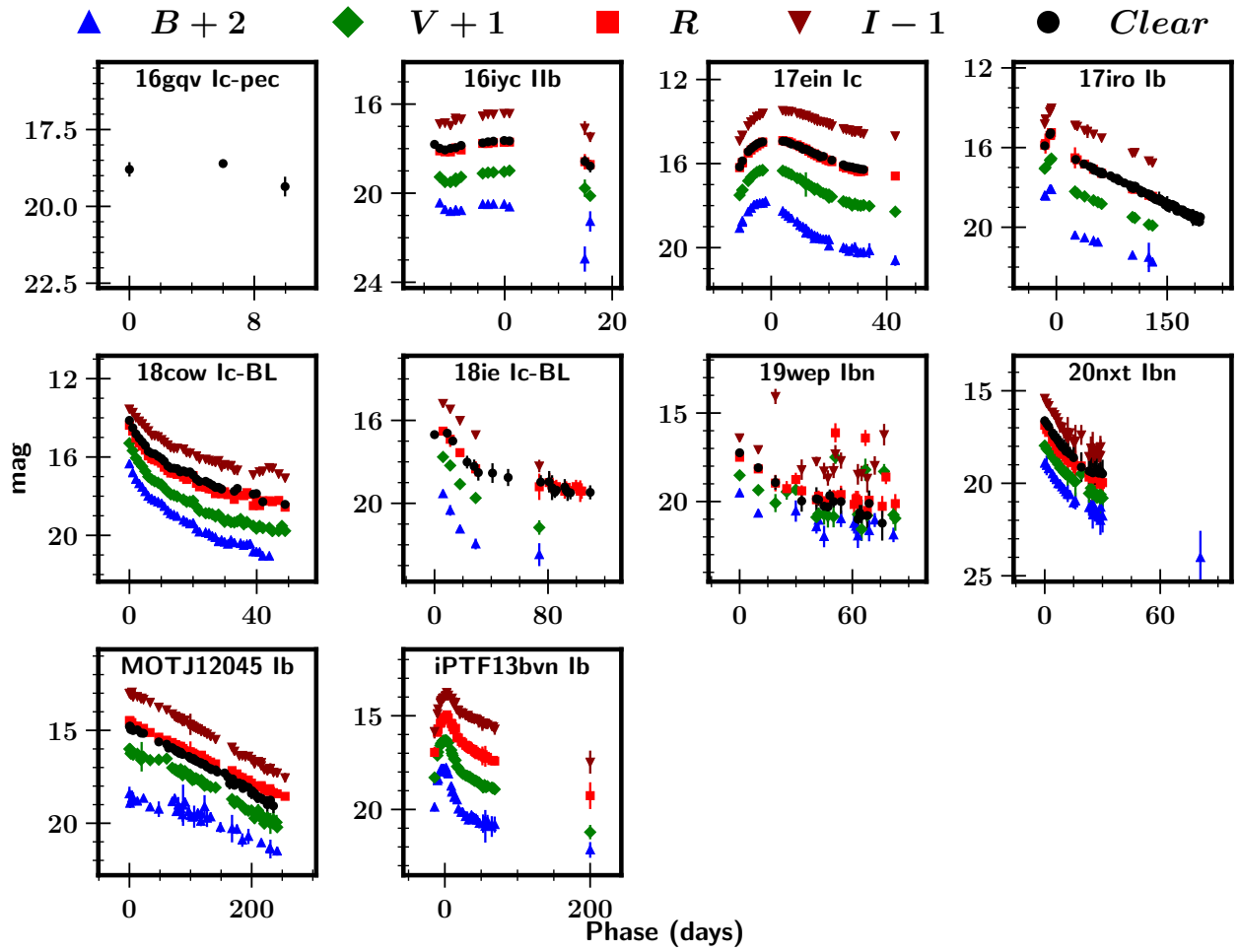


Figure A1. Continued.

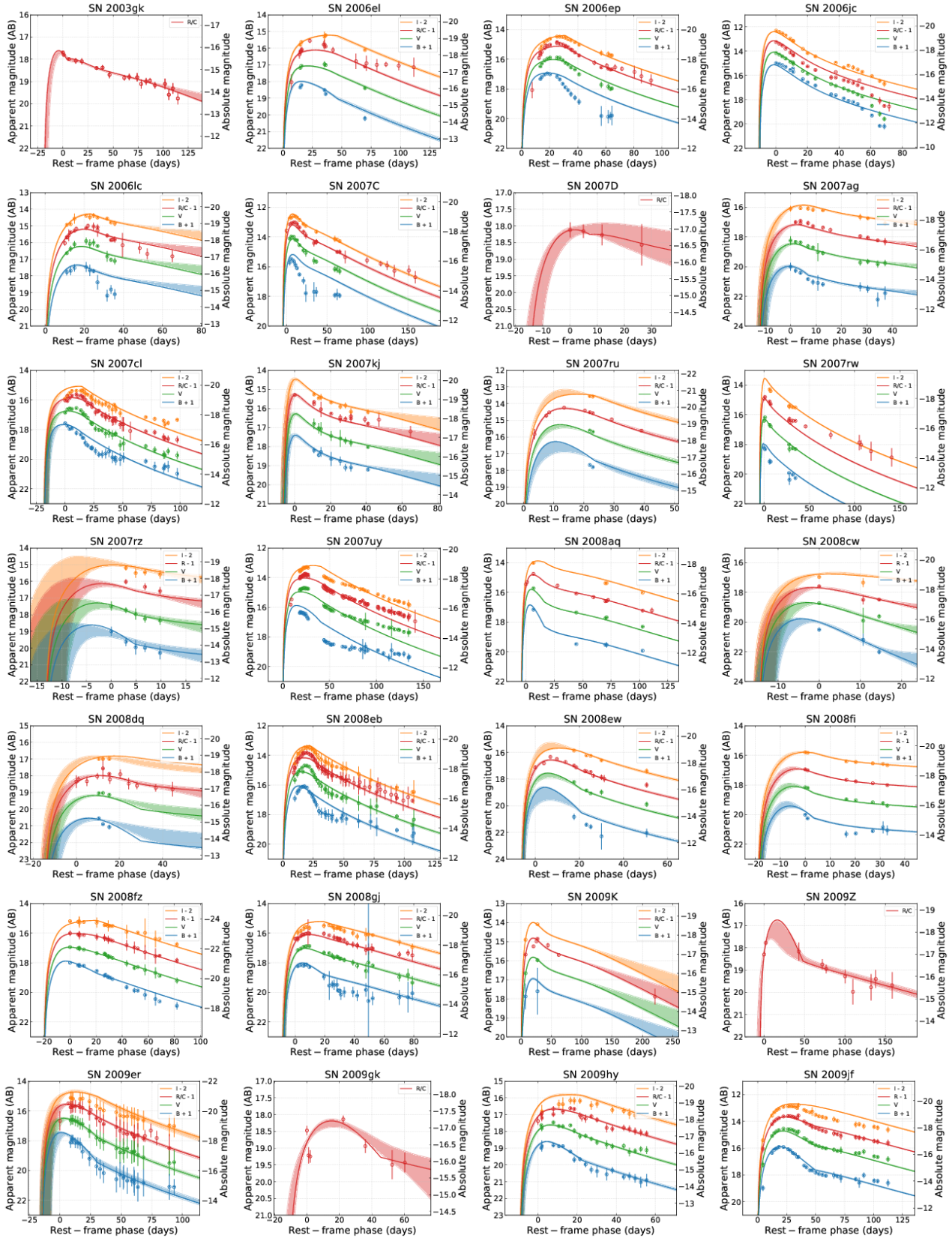


Figure A2. Model fitting of the 69 SNe with ^{56}Ni model. The shaded regions present the 1σ error region of the whole fitting area.

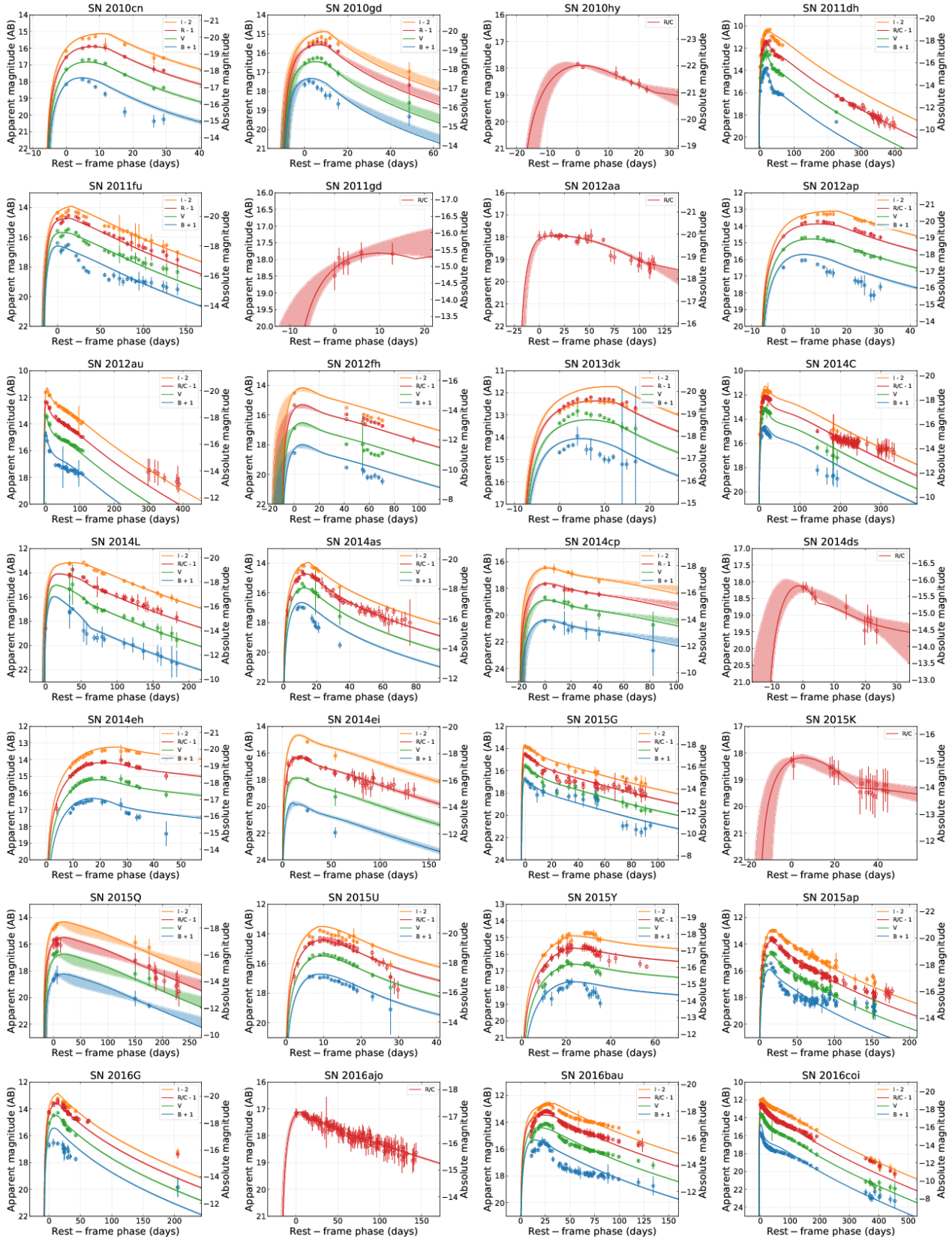


Figure A2. Continued.

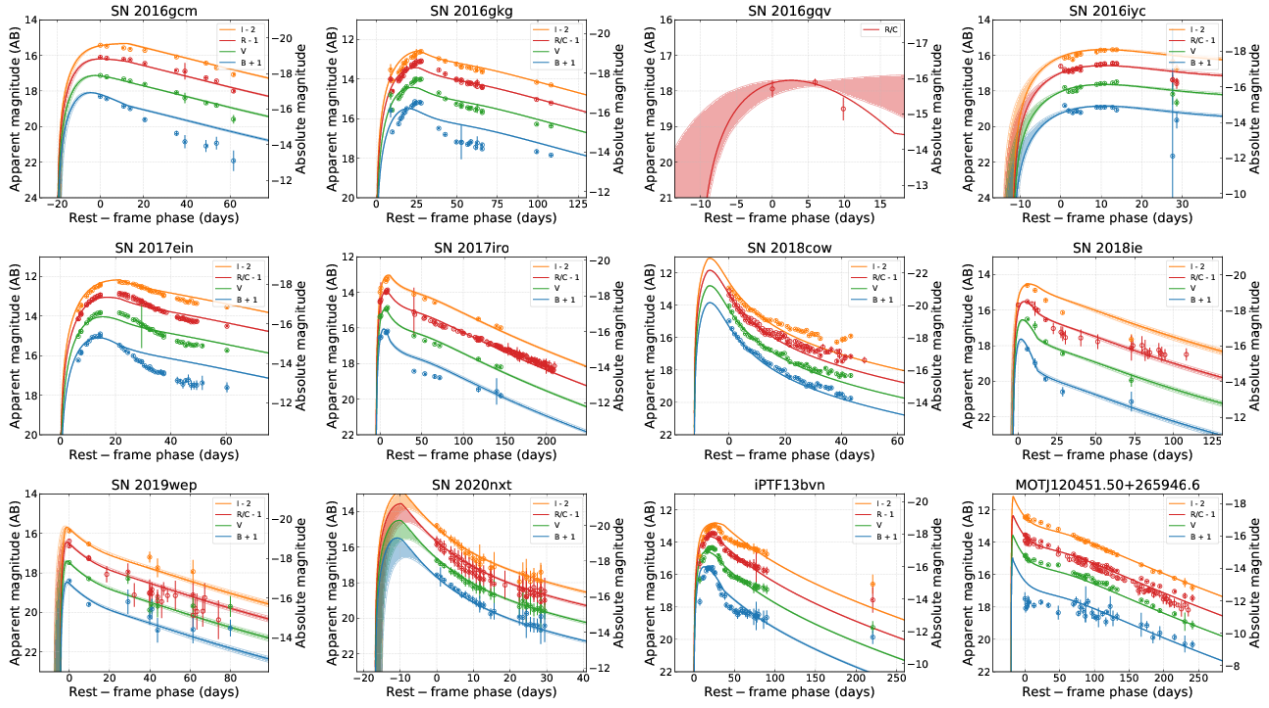


Figure A2. Continued.

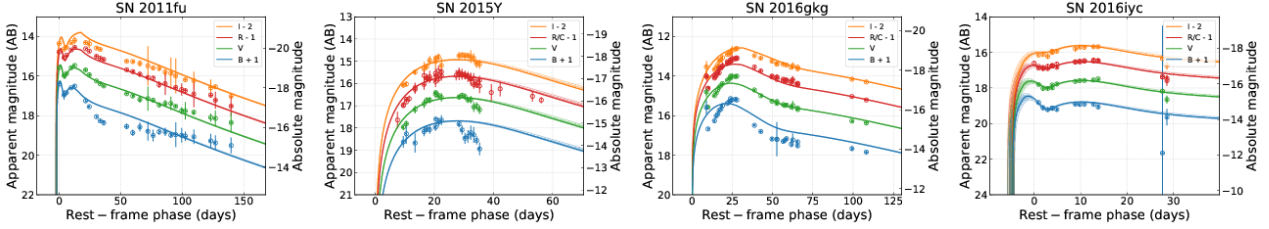


Figure A3. Model fitting of the four SNe with the cooling model

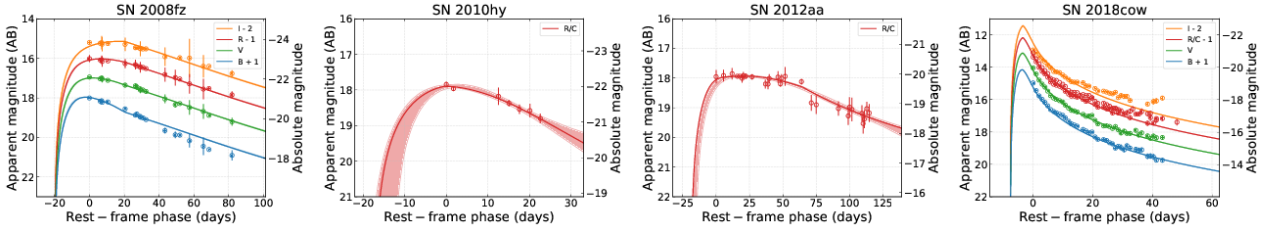


Figure A4. Model fitting of the four SNe with the magnetar model

Table A1. Best-fitting parameters of the ^{56}Ni model for the SNe.

Name	M_{ej} (M_{\odot})	v_9 (10^9 cm s^{-1})	M_{Ni} (M_{\odot})	$\log(\kappa_{\gamma}, \text{Ni})$ $\text{cm}^2 \text{ g}^{-1}$	T_{f} (10^3 K)	t_{shift} (days)	χ^2/dof
SN 2003gk	$29.11^{+7.11}_{-7.00}$ (25.04)	$4.61^{+0.72}_{-1.10}$ (3.99)	$0.17^{+0.04}_{-0.04}$ (0.15)	$-0.47^{+2.87}_{-0.43}$ (-0.23)	$2.64^{+0.19}_{-0.11}$ (2.57)	$-18.66^{+2.23}_{-1.71}$ (-17.55)	0.45 (0.63)
SN 2006el	$0.11^{+0.01}_{-0.02}$ (0.12)	$0.34^{+0.01}_{-0.01}$ (0.34)	$0.22^{+0.01}_{-0.01}$ (0.22)	$-1.19^{+0.09}_{-0.17}$ (-1.25)	$6.22^{+0.34}_{-0.29}$ (6.18)	—	6.18 (6.24)
SN 2006ep	$0.10^{+0.01}_{-0.01}$ (0.10)	$0.36^{+0.01}_{-0.01}$ (0.36)	$0.52^{+0.01}_{-0.02}$ (0.52)	$-1.51^{+0.03}_{-0.03}$ (-1.53)	$9.41^{+0.22}_{-0.22}$ (9.48)	—	11.38 (11.40)
SN 2006jc	$1.41^{+0.52}_{-0.65}$ (1.84)	$2.90^{+0.93}_{-1.28}$ (3.67)	$0.15^{+0.01}_{-0.01}$ (0.16)	$-1.13^{+0.11}_{-0.19}$ (-1.06)	$10.00^{+0.01}_{-0.01}$ (10.00)	$-10.48^{+0.45}_{-0.49}$ (-10.69)	104.49 (104.72)
SN 2006lc	$1.20^{+0.22}_{-0.19}$ (1.28)	$0.64^{+0.04}_{-0.04}$ (0.64)	$0.18^{+0.01}_{-0.01}$ (0.18)	$-1.50^{+2.55}_{-1.74}$ (0.23)	$7.44^{+0.29}_{-0.28}$ (7.36)	—	2.75 (2.86)
SN 2007C	$4.04^{+1.09}_{-1.45}$ (3.65)	$4.03^{+1.03}_{-1.45}$ (3.57)	$0.14^{+0.01}_{-0.01}$ (0.14)	$-0.50^{+0.13}_{-0.22}$ (-0.58)	$9.93^{+0.05}_{-0.10}$ (9.98)	$-4.47^{+0.43}_{-0.51}$ (-4.56)	9.94 (9.96)
SN 2007D	$14.30^{+18.13}_{-14.61}$ (22.76)	$2.49^{+1.28}_{-1.45}$ (3.13)	$0.18^{+0.20}_{-0.08}$ (0.19)	$3.06^{+1.87}_{-1.88}$ (1.26)	$4.82^{+3.78}_{-2.35}$ (3.55)	$-15.98^{+3.85}_{-2.57}$ (-16.40)	—
SN 2007ag	$2.18^{+0.24}_{-0.21}$ (2.03)	$1.17^{+0.17}_{-0.16}$ (1.22)	$0.058^{+0.004}_{-0.003}$ (0.056)	$-1.27^{+2.24}_{-1.98}$ (0.71)	$4.67^{+0.09}_{-0.09}$ (4.68)	$-12.15^{+1.64}_{-2.06}$ (-11.48)	2.13 (2.20)
SN 2007cl	$0.12^{+0.07}_{-0.03}$ (0.15)	$0.46^{+0.06}_{-0.04}$ (0.48)	$0.58^{+0.06}_{-0.08}$ (0.54)	$-1.37^{+0.13}_{-0.09}$ (-1.44)	$8.15^{+0.13}_{-0.13}$ (8.17)	$-18.26^{+2.42}_{-1.55}$ (-17.34)	6.96 (7.02)
SN 2007kj	$0.91^{+0.53}_{-0.35}$ (0.67)	$3.86^{+0.85}_{-1.07}$ (3.80)	$0.17^{+0.02}_{-0.01}$ (0.17)	$0.19^{+1.71}_{-1.41}$ (1.50)	$8.92^{+0.32}_{-0.29}$ (8.93)	$-6.31^{+1.44}_{-2.03}$ (-6.07)	2.08 (2.17)
SN 2007ru	$0.65^{+4.61}_{-0.18}$ (0.75)	$1.42^{+2.43}_{-0.05}$ (1.46)	$0.49^{+0.03}_{-0.05}$ (0.46)	$-1.25^{+0.13}_{-0.11}$ (-1.21)	$6.09^{+0.15}_{-0.71}$ (5.92)	—	38.59 (39.35)
SN 2007rw	$0.71^{+0.05}_{-0.05}$ (0.74)	$4.99^{+0.03}_{-0.07}$ (4.96)	$0.040^{+0.001}_{-0.001}$ (0.040)	$0.0097^{+0.049}_{-0.050}$ (-0.021)	$4.95^{+0.03}_{-0.03}$ (4.95)	$-4.80^{+0.12}_{-0.14}$ (-4.88)	33.39 (33.47)
SN 2007rz	$0.78^{+2.07}_{-0.84}$ (1.31)	$1.06^{+1.38}_{-2.11}$ (3.10)	$0.043^{+0.01}_{-0.01}$ (0.047)	$1.40^{+2.08}_{-1.84}$ (0.92)	$4.96^{+0.28}_{-0.44}$ (4.75)	$-13.29^{+5.06}_{-3.81}$ (-14.55)	1.45 (1.80)
SN 2007uy	$0.15^{+0.01}_{-0.01}$ (0.15)	$0.33^{+0.01}_{-0.01}$ (0.33)	$0.16^{+0.01}_{-0.01}$ (0.16)	$-1.57^{+0.02}_{-0.01}$ (-1.56)	$6.17^{+0.05}_{-0.05}$ (6.17)	—	61.42 (61.43)
SN 2008aq	$0.12^{+0.03}_{-0.02}$ (0.13)	$0.64^{+0.02}_{-0.02}$ (0.63)	$0.032^{+0.001}_{-0.001}$ (0.032)	$-0.29^{+0.10}_{-0.10}$ (-0.34)	$5.12^{+0.04}_{-0.04}$ (5.13)	$-3.84^{+0.23}_{-0.28}$ (-3.96)	34.25 (34.25)
SN 2008cw	$0.41^{+0.32}_{-0.29}$ (0.56)	$0.74^{+0.19}_{-0.08}$ (0.79)	$0.081^{+0.007}_{-0.008}$ (0.080)	$0.44^{+1.84}_{-1.83}$ (1.30)	$3.26^{+1.38}_{-1.54}$ (3.73)	$-14.45^{+2.95}_{-2.35}$ (-13.73)	7.46 (7.85)
SN 2008dq	$2.95^{+8.87}_{-8.27}$ (11.12)	$0.52^{+1.46}_{-2.49}$ (3.01)	$0.097^{+0.01}_{-0.10}$ (0.089)	$0.84^{+1.94}_{-1.94}$ (1.15)	$6.15^{+0.19}_{-1.77}$ (4.45)	$-14.69^{+3.21}_{-3.81}$ (-13.28)	2.63 (3.16)
SN 2008eb	$0.35^{+0.07}_{-0.07}$ (0.32)	$0.60^{+0.03}_{-0.03}$ (0.59)	$0.22^{+0.01}_{-0.01}$ (0.23)	$-1.57^{+0.04}_{-0.01}$ (-1.56)	$8.02^{+0.22}_{-0.21}$ (8.02)	—	3.01 (3.02)
SN 2008ew	$0.36^{+2.76}_{-0.14}$ (0.36)	$0.73^{+2.14}_{-0.07}$ (0.76)	$0.090^{+0.006}_{-0.005}$ (0.088)	$-1.54^{+0.25}_{-0.10}$ (-1.44)	$4.87^{+0.14}_{-0.11}$ (4.84)	$-5.94^{+0.74}_{-0.86}$ (-5.70)	4.91 (5.12)
SN 2008fi	$1.82^{+0.40}_{-0.75}$ (1.74)	$1.10^{+0.08}_{-0.05}$ (1.12)	$0.11^{+0.01}_{-0.01}$ (0.11)	$2.47^{+1.72}_{-1.72}$ (1.47)	$5.13^{+0.06}_{-0.06}$ (5.13)	$-18.83^{+1.31}_{-0.77}$ (-18.50)	8.63 (8.76)
SN 2008fz	$2.43^{+0.29}_{-0.28}$ (2.46)	$2.59^{+0.03}_{-0.03}$ (2.60)	$17.52^{+0.18}_{-0.18}$ (17.44)	$-0.73^{+0.05}_{-0.05}$ (-0.73)	$7.41^{+0.05}_{-0.05}$ (7.41)	$-19.97^{+0.13}_{-0.06}$ (-19.92)	7.10 (7.12)
SN 2008gj	$0.40^{+0.13}_{-0.17}$ (0.39)	$0.61^{+0.05}_{-0.04}$ (0.62)	$0.21^{+0.01}_{-0.01}$ (0.20)	$-1.15^{+0.32}_{-0.18}$ (-1.11)	$6.77^{+0.17}_{-0.17}$ (6.75)	$-8.10^{+1.19}_{-1.00}$ (-7.90)	2.92 (2.93)
SN 2009K	$12.37^{+3.76}_{-5.29}$ (12.40)	$3.51^{+1.06}_{-1.50}$ (3.52)	$0.11^{+0.01}_{-0.01}$ (0.11)	$-0.20^{+2.10}_{-1.21}$ (0.91)	$8.86^{+0.29}_{-0.26}$ (8.83)	—	8.47 (8.80)
SN 2009Z	$27.09^{+20.69}_{-11.65}$ (16.55)	$3.30^{+1.12}_{-1.37}$ (3.36)	$0.77^{+0.38}_{-0.26}$ (0.44)	$2.68^{+1.61}_{-1.62}$ (1.63)	$3.03^{+4.18}_{-0.44}$ (2.61)	$-5.68^{+1.64}_{-3.28}$ (-6.56)	0.59 (1.35)
SN 2009er	$1.02^{+1.33}_{-0.54}$ (0.89)	$1.07^{+0.49}_{-0.26}$ (1.27)	$1.27^{+0.37}_{-0.26}$ (1.11)	$-1.45^{+0.40}_{-0.22}$ (-1.27)	$5.33^{+0.53}_{-0.43}$ (5.13)	$-14.51^{+4.34}_{-4.94}$ (-11.99)	0.38 (0.42)
SN 2009gk	$14.85^{+13.87}_{-15.34}$ (29.67)	$1.23^{+1.64}_{-0.66}$ (1.70)	$0.24^{+0.14}_{-0.15}$ (0.32)	$-0.99^{+2.10}_{-2.04}$ (0.91)	$2.65^{+2.21}_{-1.01}$ (3.06)	$-12.22^{+2.96}_{-3.33}$ (-13.38)	23.75 (32.35)
SN 2009hy	$0.47^{+0.12}_{-0.13}$ (0.42)	$0.57^{+0.05}_{-0.05}$ (0.60)	$0.19^{+0.01}_{-0.01}$ (0.19)	$-1.54^{+0.17}_{-0.07}$ (-1.48)	$6.04^{+0.25}_{-0.24}$ (6.02)	$-9.22^{+0.90}_{-0.79}$ (-8.63)	1.89 (1.92)
SN 2009jf	$1.96^{+0.07}_{-0.07}$ (1.97)	$0.63^{+0.01}_{-0.01}$ (0.63)	$0.23^{+0.01}_{-0.01}$ (0.23)	$-1.57^{+0.01}_{-0.01}$ (-1.56)	$4.57^{+0.05}_{-0.05}$ (4.57)	—	7.81 (7.82)
SN 2010cn	$0.26^{+0.06}_{-0.07}$ (0.22)	$0.95^{+0.06}_{-0.05}$ (0.98)	$0.40^{+0.02}_{-0.02}$ (0.40)	$-1.50^{+0.21}_{-0.12}$ (-1.40)	$8.05^{+0.48}_{-0.46}$ (8.04)	$-6.00^{+0.52}_{-0.42}$ (-5.71)	7.43 (7.44)
SN 2010gd	$0.11^{+0.11}_{-0.03}$ (0.14)	$0.60^{+0.17}_{-0.09}$ (0.66)	$0.60^{+0.11}_{-0.12}$ (0.49)	$-1.53^{+0.29}_{-0.08}$ (-1.46)	$9.86^{+0.11}_{-0.27}$ (9.95)	$-10.33^{+1.92}_{-1.98}$ (-10.05)	5.36 (5.56)
SN 2010hy	$12.75^{+14.45}_{-9.36}$ (12.50)	$4.84^{+2.06}_{-2.16}$ (6.97)	$10.91^{+1.66}_{-1.18}$ (10.62)	$0.48^{+1.76}_{-1.79}$ (1.43)	$6.10^{+2.79}_{-3.36}$ (4.67)	$-19.12^{+3.13}_{-1.90}$ (-17.35)	1.91 (15.08)
SN 2011dh	$1.49^{+0.05}_{-0.05}$ (1.48)	$0.53^{+0.01}_{-0.01}$ (0.53)	$0.077^{+0.001}_{-0.001}$ (0.077)	$-1.57^{+0.01}_{-0.01}$ (-1.56)	$4.28^{+0.03}_{-0.03}$ (4.28)	$-4.10^{+0.07}_{-0.07}$ (-4.09)	8.78 (8.78)
SN 2011fu	$0.44^{+0.09}_{-0.08}$ (0.47)	$0.64^{+0.04}_{-0.04}$ (0.61)	$0.97^{+0.05}_{-0.05}$ (1.00)	$-1.12^{+0.14}_{-0.14}$ (-1.19)	$8.61^{+0.16}_{-0.16}$ (8.58)	$-16.24^{+1.52}_{-1.72}$ (-17.01)	16.12 (16.12)
SN 2011gd	$33.48^{+11.73}_{-16.03}$ (33.34)	$2.37^{+2.16}_{-1.18}$ (1.49)	$0.14^{+0.22}_{-0.08}$ (0.12)	$0.34^{+1.91}_{-1.86}$ (1.20)	$5.22^{+3.48}_{-2.75}$ (2.78)	$-9.94^{+4.45}_{-3.85}$ (-14.18)	—

Table A1. ...continued.

Name	M_{ej} (M_{\odot})	v_9 (10^9 cm s^{-1})	M_{Ni} (M_{\odot})	$\log(\kappa_{\gamma}, Ni)$ $\text{cm}^2 \text{ g}^{-1}$	T_f (10^3 K)	t_{shift} (days)	χ^2/dof
SN 2012aa	$1.33^{+0.98}_{-0.73}(1.30)$	$0.84^{+0.05}_{-0.05}(0.84)$	$2.96^{+0.11}_{-0.10}(2.93)$	$3.17^{+1.61}_{-1.64}(1.63)$	$3.19^{+0.99}_{-1.48}(4.05)$	$-19.34^{+2.56}_{-1.54}(-17.87)$	0.79 (0.86)
SN 2012ap	$0.42^{+0.08}_{-0.09}(0.37)$	$0.85^{+0.03}_{-0.03}(0.86)$	$0.74^{+0.05}_{-0.04}(0.75)$	$-1.55^{+0.10}_{-0.05}(-1.51)$	$8.08^{+0.22}_{-0.22}(8.10)$	$-7.08^{+0.37}_{-0.29}(-6.88)$	6.92 (6.98)
SN 2012au	$0.37^{+0.02}_{-0.02}(0.37)$	$2.77^{+0.07}_{-0.06}(2.76)$	$0.13^{+0.01}_{-0.01}(0.13)$	$0.63^{+0.04}_{-0.04}(0.63)$	$5.69^{+0.02}_{-0.02}(5.68)$	$-5.13^{+0.13}_{-0.13}(-5.15)$	32.89 (32.89)
SN 2012fh	$5.53^{+7.02}_{-6.05}(11.53)$	$2.65^{+0.99}_{-1.42}(3.63)$	$0.0028^{+0.0002}_{-0.0002}(0.0029)$	$-0.89^{+0.23}_{-0.22}(-0.97)$	$5.97^{+0.06}_{-0.06}(5.97)$	$-9.82^{+5.35}_{-3.78}(-14.68)$	42.34 (46.11)
SN 2013dk	$0.10^{+0.01}_{-0.01}(0.10)$	$0.67^{+0.02}_{-0.02}(0.68)$	$0.98^{+0.02}_{-0.02}(0.98)$	$-1.57^{+0.01}_{-0.01}(-1.57)$	$9.97^{+0.02}_{-0.05}(9.99)$	$-8.12^{+0.35}_{-0.37}(-8.10)$	33.03 (33.09)
SN 2014C	$1.32^{+0.05}_{-0.06}(1.31)$	$0.85^{+0.02}_{-0.02}(0.85)$	$0.094^{+0.001}_{-0.001}(0.094)$	$-0.67^{+0.03}_{-0.03}(-0.67)$	$7.55^{+0.07}_{-0.08}(7.55)$	—	12.07 (12.07)
SN 2014L	$0.24^{+0.26}_{-0.21}(0.41)$	$0.50^{+0.02}_{-0.03}(0.48)$	$0.25^{+0.01}_{-0.01}(0.25)$	$-0.95^{+0.31}_{-0.23}(-1.20)$	$4.21^{+0.09}_{-0.08}(4.21)$	$-1.45^{+1.07}_{-2.25}(-2.47)$	3.62 (3.63)
SN 2014as	$0.32^{+0.03}_{-0.03}(0.32)$	$0.83^{+0.02}_{-0.02}(0.83)$	$0.24^{+0.01}_{-0.01}(0.24)$	$-1.57^{+0.01}_{-0.01}(-1.56)$	$9.15^{+0.20}_{-0.19}(9.14)$	—	7.22 (7.24)
SN 2014cp	$15.47^{+4.56}_{-5.04}(11.56)$	$4.17^{+1.07}_{-1.50}(3.50)$	$0.029^{+0.001}_{-0.001}(0.029)$	$-0.63^{+1.91}_{-1.83}(1.19)$	$5.88^{+0.24}_{-0.22}(5.93)$	$-19.20^{+2.24}_{-1.36}(-18.11)$	0.76 (0.81)
SN 2014ds	$8.42^{+30.48}_{-6.02}(7.61)$	$4.15^{+1.05}_{-1.23}(3.47)$	$0.067^{+0.145}_{-0.030}(0.053)$	$-0.37^{+1.92}_{-1.87}(1.19)$	$3.06^{+4.81}_{-3.11}(2.77)$	$-11.89^{+4.03}_{-3.03}(-15.61)$	0.40 (4.45)
SN 2014eh	$1.69^{+0.11}_{-0.11}(1.68)$	$0.79^{+0.02}_{-0.02}(0.78)$	$0.31^{+0.01}_{-0.01}(0.31)$	$-1.34^{+2.18}_{-2.15}(0.80)$	$6.77^{+0.11}_{-0.11}(6.75)$	—	3.42 (3.43)
SN 2014ei	$5.55^{+2.07}_{-1.59}(6.68)$	$2.41^{+1.32}_{-0.91}(3.07)$	$0.084^{+0.007}_{-0.006}(0.083)$	$-0.92^{+0.20}_{-0.22}(-0.76)$	$4.15^{+0.17}_{-0.16}(4.15)$	—	0.81 (0.83)
SN 2015G	$0.10^{+0.02}_{-0.01}(0.11)$	$4.76^{+0.29}_{-0.55}(4.61)$	$0.015^{+0.001}_{-0.001}(0.015)$	$1.03^{+0.08}_{-0.13}(0.94)$	$8.00^{+0.10}_{-0.09}(8.00)$	$-2.76^{+0.25}_{-0.34}(-2.93)$	2.20 (2.22)
SN 2015K	$30.19^{+22.11}_{-7.42}(11.59)$	$1.95^{+1.22}_{-1.52}(3.31)$	$0.11^{+0.104}_{-0.011}(0.027)$	$3.06^{+1.89}_{-1.92}(1.21)$	$3.46^{+4.66}_{-3.21}(2.30)$	$-15.15^{+5.30}_{-3.51}(-15.12)$	0.11 (0.45)
SN 2015Q	$29.61^{+17.37}_{-11.09}(21.24)$	$2.51^{+1.18}_{-1.28}(3.26)$	$0.080^{+0.028}_{-0.013}(0.057)$	$-1.06^{+2.65}_{-0.72}(-0.38)$	$5.84^{+0.26}_{-0.24}(5.86)$	$-18.36^{+3.26}_{-2.59}(-16.12)$	0.84 (0.87)
SN 2015U	$1.30^{+0.26}_{-0.18}(1.31)$	$2.40^{+0.26}_{-0.17}(2.43)$	$0.24^{+0.01}_{-0.01}(0.24)$	$-1.47^{+0.07}_{-0.06}(-1.45)$	$7.69^{+0.13}_{-0.13}(7.70)$	—	6.01 (6.02)
SN 2015Y	$1.07^{+0.09}_{-0.10}(1.07)$	$0.23^{+0.01}_{-0.01}(0.23)$	$0.073^{+0.002}_{-0.003}(0.072)$	$3.11^{+1.89}_{-1.89}(1.21)$	$9.73^{+0.18}_{-0.27}(9.91)$	—	2.82 (2.82)
SN 2015ap	$1.29^{+0.04}_{-0.04}(1.29)$	$1.29^{+0.01}_{-0.01}(1.29)$	$0.42^{+0.01}_{-0.01}(0.42)$	$-1.26^{+0.01}_{-0.01}(-1.26)$	$7.42^{+0.04}_{-0.04}(7.42)$	—	11.96 (11.96)
SN 2016G	$0.50^{+0.07}_{-0.10}(0.45)$	$0.63^{+0.02}_{-0.02}(0.64)$	$0.58^{+0.01}_{-0.01}(0.58)$	$-1.55^{+0.12}_{-0.05}(-1.50)$	$9.99^{+0.01}_{-0.02}(10.00)$	$-8.09^{+0.46}_{-0.35}(-7.90)$	15.81 (15.85)
SN 2016ajo	$21.13^{+8.20}_{-9.21}(22.79)$	$2.14^{+1.04}_{-1.43}(3.52)$	$0.27^{+0.14}_{-0.04}(0.18)$	$2.03^{+1.50}_{-1.52}(1.78)$	$5.28^{+3.45}_{-2.07}(3.37)$	$-17.26^{+2.31}_{-1.11}(-18.49)$	0.18 (1.60)
SN 2016bau	$0.10^{+0.01}_{-0.01}(0.10)$	$0.29^{+0.01}_{-0.01}(0.29)$	$0.12^{+0.01}_{-0.01}(0.12)$	$-1.46^{+0.02}_{-0.04}(-1.47)$	$7.03^{+0.11}_{-0.11}(7.03)$	—	15.47 (15.47)
SN 2016coi	$0.10^{+0.01}_{-0.01}(0.10)$	$1.30^{+0.01}_{-0.01}(1.30)$	$0.077^{+0.001}_{-0.001}(0.077)$	$0.53^{+0.01}_{-0.01}(0.53)$	$5.16^{+0.01}_{-0.01}(5.16)$	$-5.23^{+0.03}_{-0.04}(-5.22)$	180.05 (180.06)
SN 2016gcm	$0.49^{+0.12}_{-0.14}(0.43)$	$0.52^{+0.02}_{-0.02}(0.54)$	$0.27^{+0.01}_{-0.01}(0.27)$	$-1.45^{+0.20}_{-0.12}(-1.38)$	$6.90^{+0.17}_{-0.17}(6.90)$	$-19.81^{+0.89}_{-0.50}(-19.31)$	9.93 (9.96)
SN 2016gkg	$1.05^{+0.03}_{-0.03}(1.06)$	$0.41^{+0.01}_{-0.01}(0.41)$	$0.16^{+0.01}_{-0.01}(0.16)$	$-1.57^{+0.01}_{-0.01}(-1.57)$	$8.16^{+0.06}_{-0.06}(8.16)$	—	55.79 (55.80)
SN 2016gqv	$11.50^{+17.51}_{-16.44}(24.42)$	$3.26^{+1.31}_{-1.72}(3.11)$	$0.086^{+0.12}_{-0.07}(0.11)$	$1.94^{+1.91}_{-1.88}(1.20)$	$3.14^{+4.80}_{-3.44}(2.40)$	$-10.54^{+4.58}_{-3.44}(-15.11)$	—
SN 2016iyC	$3.82^{+1.32}_{-1.71}(3.62)$	$0.84^{+0.24}_{-0.43}(0.77)$	$0.058^{+0.004}_{-0.003}(0.060)$	$0.94^{+1.90}_{-1.89}(1.21)$	$7.85^{+0.17}_{-0.27}(7.88)$	$-11.87^{+1.11}_{-1.91}(-12.55)$	2.75 (2.88)
SN 2017ein	$0.39^{+0.01}_{-0.01}(0.38)$	$0.37^{+0.01}_{-0.01}(0.37)$	$0.050^{+0.001}_{-0.001}(0.050)$	$-1.57^{+0.01}_{-0.01}(-1.57)$	$7.28^{+0.04}_{-0.04}(7.30)$	—	37.98 (37.99)
SN 2017iro	$0.37^{+0.02}_{-0.02}(0.37)$	$0.90^{+0.02}_{-0.02}(0.90)$	$0.081^{+0.001}_{-0.001}(0.081)$	$-0.48^{+0.04}_{-0.04}(-0.48)$	$6.40^{+0.28}_{-0.27}(6.35)$	$-4.75^{+0.14}_{-0.14}(-4.78)$	16.01 (16.02)
SN 2018cow	$2.56^{+0.03}_{-0.03}(2.56)$	$10.00^{+0.01}_{-0.01}(10.00)$	$3.57^{+0.04}_{-0.03}(3.56)$	$-1.57^{+0.01}_{-0.01}(-1.57)$	$10.00^{+0.01}_{-0.01}(10.00)$	$-12.43^{+0.03}_{-0.03}(-12.42)$	241.67 (241.69)
SN 2018ie	$0.15^{+0.13}_{-0.11}(0.25)$	$1.70^{+0.12}_{-0.13}(1.59)$	$0.077^{+0.003}_{-0.003}(0.079)$	$0.057^{+0.32}_{-0.28}(-0.24)$	$4.62^{+0.15}_{-0.13}(4.63)$	$-3.34^{+0.63}_{-0.78}(-3.97)$	6.63 (6.65)
SN 2019wep	$0.17^{+0.29}_{-0.13}(0.27)$	$3.86^{+0.83}_{-1.17}(3.84)$	$0.10^{+0.01}_{-0.01}(0.11)$	$0.67^{+0.38}_{-0.38}(0.35)$	$9.77^{+0.17}_{-0.28}(9.92)$	$-4.56^{+1.51}_{-1.81}(-5.77)$	1.70 (1.78)
SN 2020nxt	$0.65^{+0.69}_{-0.31}(0.50)$	$4.39^{+0.62}_{-1.06}(4.15)$	$1.41^{+0.64}_{-0.43}(0.94)$	$-1.47^{+0.32}_{-0.15}(-1.37)$	$9.92^{+0.06}_{-0.12}(9.98)$	$-16.84^{+1.00}_{-0.82}(-16.15)$	0.47 (1.36)
iPTF13bvn	$0.15^{+0.01}_{-0.01}(0.15)$	$0.37^{+0.01}_{-0.01}(0.37)$	$0.11^{+0.01}_{-0.01}(0.11)$	$-1.57^{+0.01}_{-0.01}(-1.57)$	$5.59^{+0.10}_{-0.10}(5.57)$	—	10.14 (10.15)
MOTJ120451.50+265946.6	$0.11^{+0.04}_{-0.02}(0.12)$	$4.57^{+0.44}_{-0.80}(4.39)$	$0.015^{+0.001}_{-0.001}(0.015)$	$1.82^{+0.13}_{-0.19}(1.70)$	$5.69^{+0.03}_{-0.03}(5.69)$	$-20.00^{+0.02}_{-0.01}(-19.99)$	15.53 (16.03)

Table A2. Best-fitting parameters of the cooling plus ^{56}Ni model for the double-peaked SNe.

Name	M_e (M_\odot)	$R_{e,12}$ (10^{12} cm)	$E_{e,50}$ ($10^{50} \text{ erg s}^{-1}$)	M_{ej} (M_\odot)	v_9 (10^9 cm s^{-1})	M_{Ni} (M_\odot)	$\log(\kappa_\gamma)$ $\text{cm}^2 \text{ g}^{-1}$	T_f (10^3 K)	t_{shift} (days)	χ^2/dof
SN 2011fu	$0.059^{+0.009}_{-0.008}$ (0.054)	$103.83^{+135.3}_{-68.4}$ (156.23)	$0.54^{+0.24}_{-0.23}$ (0.37)	$0.68^{+0.13}_{-0.13}$ (0.78)	$1.18^{+0.04}_{-0.04}$ (1.18)	$0.60^{+0.01}_{-0.01}$ (0.61)	$-0.66^{+0.09}_{-0.08}$ (-0.72)	$8.05^{+0.13}_{-0.13}$ (8.08)	$-2.07^{+0.41}_{-0.43}$ (-2.36)	10.27 (10.28)
SN 2015Y	$19.10^{+8.96}_{-10.15}$ (17.03)	$386.05^{+1104.94}_{-983.49}$ (1347.86)	$-4.65^{+0.72}_{-0.54}$ (-4.22)	$37.51^{+1.82}_{-1.99}$ (37.00)	$4.97^{+0.09}_{-0.19}$ (4.88)	$0.087^{+0.003}_{-0.003}$ (0.086)	$-1.57^{+0.02}_{-0.01}$ (-1.56)	$9.90^{+0.14}_{-0.20}$ (9.80)	—	5.14 (5.17)
SN 2016gkg	$0.21^{+0.01}_{-0.01}$ (0.21)	$2996.83^{+9.06}_{-19.66}$ (2987.88)	$-1.80^{+0.01}_{-0.01}$ (-1.80)	$1.09^{+0.04}_{-0.04}$ (1.09)	$0.30^{+0.01}_{-0.01}$ (0.30)	$0.11^{+0.01}_{-0.01}$ (0.11)	$-1.57^{+0.01}_{-0.01}$ (-1.57)	$7.62^{+0.07}_{-0.07}$ (7.62)	—	41.55 (41.57)
SN 2016iyc	$0.011^{+0.002}_{-0.001}$ (0.011)	$422.40^{+327.06}_{-205.44}$ (436.80)	$-1.88^{+0.20}_{-0.17}$ (-1.89)	$1.16^{+0.38}_{-0.16}$ (1.26)	$0.70^{+0.24}_{-0.09}$ (0.68)	$0.042^{+0.002}_{-0.002}$ (0.043)	$1.41^{+1.94}_{-1.91}$ (1.16)	$7.90^{+0.19}_{-0.19}$ (7.83)	$-4.64^{+0.67}_{-0.76}$ (-4.98)	1.10 (1.12)

Table A3. Best-fitting parameters of the magnetar model for the luminous SNe.

Name	M_{ej} (M_\odot)	P_0 (ms)	$B_{P,14}$ (10^{14} G)	V_9 (10^9 cm s^{-1})	$\log(\kappa_\gamma)$ $\text{cm}^2 \text{ g}^{-1}$	T_f (10^3 K)	t_{shift} (days)	χ^2
SN 2008fz	$1.93^{+0.31}_{-0.37}$ (1.86)	$2.99^{+0.01}_{-0.01}$ (2.99)	$1.13^{+0.02}_{-0.02}$ (1.14)	$2.63^{+0.03}_{-0.03}$ (2.63)	$-0.25^{+0.10}_{-0.07}$ (-0.23)	$7.43^{+0.05}_{-0.05}$ (7.42)	$-19.99^{+0.08}_{-0.04}$ (-19.95)	8.01
SN 2010hy	$39.35^{+13.83}_{-24.71}$ (31.26)	$2.55^{+0.61}_{-1.40}$ (3.27)	$3.91^{+1.64}_{-1.23}$ (3.19)	$4.97^{+2.52}_{-2.12}$ (5.96)	$1.84^{+1.83}_{-1.81}$ (1.32)	$8.78^{+1.87}_{-2.14}$ (7.23)	$-17.72^{+3.40}_{-2.46}$ (-16.5)	
SN 2012aa	$0.62^{+0.31}_{-0.30}$ (0.73)	$1.13^{+1.52}_{-0.74}$ (1.81)	$2.91^{+0.15}_{-0.18}$ (2.93)	$0.36^{+0.04}_{-0.04}$ (0.38)	$2.12^{+1.66}_{-1.67}$ (1.56)	$8.24^{+2.03}_{-3.26}$ (6.36)	$-18.89^{+2.30}_{-1.34}$ (-18.17)	0.76
SN 2018cow	$1.23^{+0.02}_{-0.02}$ (1.23)	$1.22^{+0.01}_{-0.01}$ (1.23)	$0.10^{+0.01}_{-0.01}$ (0.10)	$10.0^{+0.01}_{-0.02}$ (9.99)	$-2.00^{+0.01}_{-0.01}$ (-2.00)	$10.0^{+0.01}_{-0.01}$ (10.00)	$-7.62^{+0.02}_{-0.02}$ (-7.62)	191.64

Table A4. Light-Curve Data in the Standard System (only a portion of data is shown here as an example)

SN	MJD	<i>B</i> (mag)	<i>V</i> (mag)	<i>R</i> (mag)	<i>I</i> (mag)	<i>Clear</i> (mag)
2003gk	52821.455	—	—	—	—	17.717±0.061
2003gk	52822.463	—	—	—	—	17.828±0.051
2003gk	52827.480	—	—	—	—	18.016±0.068
2003gk	52834.456	—	—	—	—	18.091±0.124
2003gk	52840.448	—	—	—	—	18.114±0.145
2003gk	52855.405	—	—	—	—	18.417±0.072
2003gk	52861.415	—	—	—	—	18.399±0.113
2003gk	52868.452	—	—	—	—	18.718±0.155
2003gk	52888.281	—	—	—	—	18.817±0.143
2003gk	52896.328	—	—	—	—	18.832±0.188
2003gk	52900.263	—	—	—	—	19.131±0.207
2003gk	52905.289	—	—	—	—	19.018±0.148
2003gk	52909.258	—	—	—	—	18.987±0.112
2003gk	52914.230	—	—	—	—	19.187±0.141
2003gk	52924.305	—	—	—	—	19.126±0.236
2003gk	52928.232	—	—	—	—	19.616±0.238
2003gk	52932.210	—	—	—	—	19.334±0.239
2003gk	52937.237	—	—	—	—	19.784±0.265
2003gk	52821.455	—	—	—	—	17.717±0.061
2003gk	52822.463	—	—	—	—	17.828±0.051
2003gk	52827.480	—	—	—	—	18.016±0.068
2003gk	52834.456	—	—	—	—	18.091±0.124
2003gk	52840.448	—	—	—	—	18.114±0.145
2003gk	52855.405	—	—	—	—	18.417±0.072
2003gk	52861.415	—	—	—	—	18.399±0.113
2003gk	52868.452	—	—	—	—	18.718±0.155
2003gk	52883.306	—	—	—	—	18.855±0.133
2003gk	52888.281	—	—	—	—	18.817±0.143
2003gk	52896.328	—	—	—	—	18.832±0.188
2003gk	52900.263	—	—	—	—	19.131±0.207
2003gk	52905.289	—	—	—	—	19.018±0.148
2003gk	52909.258	—	—	—	—	18.987±0.112
2003gk	52914.230	—	—	—	—	19.187±0.141
2003gk	52924.305	—	—	—	—	19.126±0.236
2003gk	52928.232	—	—	—	—	19.616±0.238
2003gk	52932.210	—	—	—	—	19.334±0.239
2003gk	52937.237	—	—	—	—	19.784±0.265
2003gk	52883.306	—	—	—	—	18.855±0.133

Table A4 (cont'd)

SN	MJD	<i>B</i> (mag)	<i>V</i> (mag)	<i>R</i> (mag)	<i>I</i> (mag)	<i>Clear</i> (mag)
2006el 53965.324	—	—	—	—	—	19.808±0.464
2006el 53972.281	—	—	—	—	—	18.153±0.250
2006el 53973.007	18.920±0.069	18.335±0.050	18.022±0.095	17.846±0.121	—	—
2006el 53973.304	—	—	—	—	—	17.952±0.215
2006el 53973.977	18.782±0.057	18.213±0.048	17.922±0.067	17.695±0.091	—	—
2006el 53974.304	—	—	—	—	—	17.865±0.175
2006el 53981.255	—	—	—	—	—	17.328±0.140
2006el 53993.265	—	—	—	—	—	17.563±0.215
2006el 53993.957	19.078±0.093	18.118±0.181	17.549±0.296	17.367±0.301	—	—
2006el 53994.925	19.316±0.076	18.163±0.059	17.668±0.071	17.287±0.084	—	—
2006el 54001.269	—	—	—	—	—	17.888±0.183
2006el 54021.156	—	—	—	—	—	18.561±0.462
2006el 54028.887	20.778±0.143	19.548±0.079	18.877±0.063	18.171±0.056	—	—
2006el 54030.193	—	—	—	—	—	18.679±0.456
2006el 54039.155	—	—	—	—	—	18.772±0.341
2006el 54047.126	—	—	—	—	—	18.751±0.152
2006el 54058.109	—	—	—	—	—	18.828±0.284
2006el 54071.111	—	—	—	—	—	18.917±0.579

Table A5. Light Curve Data in Natural System (only a portion of data is shown here as example)

SN	MJD	<i>B</i> (mag)	<i>V</i> (mag)	<i>R</i> (mag)	<i>I</i> (mag)	<i>Clear</i> (mag)	System
2003gk 52821.455	—	—	—	—	—	17.717±0.061	kait2
2003gk 52822.463	—	—	—	—	—	17.828±0.051	kait2
2003gk 52827.480	—	—	—	—	—	18.016±0.068	kait2
2003gk 52834.456	—	—	—	—	—	18.091±0.124	kait2
2003gk 52840.448	—	—	—	—	—	18.114±0.145	kait2
2003gk 52855.405	—	—	—	—	—	18.417±0.072	kait2
2003gk 52861.415	—	—	—	—	—	18.399±0.113	kait2
2003gk 52868.452	—	—	—	—	—	18.718±0.155	kait2
2003gk 52883.306	—	—	—	—	—	18.855±0.133	kait2
2003gk 52888.281	—	—	—	—	—	18.817±0.143	kait2
2003gk 52896.328	—	—	—	—	—	18.832±0.188	kait2
2003gk 52900.263	—	—	—	—	—	19.131±0.207	kait2
2003gk 52905.289	—	—	—	—	—	19.018±0.148	kait2
2003gk 52909.258	—	—	—	—	—	18.987±0.112	kait2
2003gk 52914.230	—	—	—	—	—	19.187±0.141	kait2
2003gk 52924.305	—	—	—	—	—	19.126±0.236	kait2
2003gk 52928.232	—	—	—	—	—	19.616±0.238	kait2
2003gk 52932.210	—	—	—	—	—	19.334±0.239	kait2
2003gk 52937.237	—	—	—	—	—	19.784±0.265	kait2
2003gk 52821.455	—	—	—	—	—	17.717±0.061	kait2
2003gk 52822.463	—	—	—	—	—	17.828±0.051	kait2
2003gk 52827.480	—	—	—	—	—	18.016±0.068	kait2
2003gk 52834.456	—	—	—	—	—	18.091±0.124	kait2
2003gk 52840.448	—	—	—	—	—	18.114±0.145	kait2
2003gk 52855.405	—	—	—	—	—	18.417±0.072	kait2
2003gk 52861.415	—	—	—	—	—	18.399±0.113	kait2
2003gk 52868.452	—	—	—	—	—	18.718±0.155	kait2
2003gk 52883.306	—	—	—	—	—	18.855±0.133	kait2
2003gk 52888.281	—	—	—	—	—	18.817±0.143	kait2
2003gk 52896.328	—	—	—	—	—	18.832±0.188	kait2
2003gk 52900.263	—	—	—	—	—	19.131±0.207	kait2
2003gk 52905.289	—	—	—	—	—	19.018±0.148	kait2
2003gk 52909.258	—	—	—	—	—	18.987±0.112	kait2
2003gk 52914.230	—	—	—	—	—	19.187±0.141	kait2
2003gk 52924.305	—	—	—	—	—	19.126±0.236	kait2
2003gk 52928.232	—	—	—	—	—	19.616±0.238	kait2
2003gk 52932.210	—	—	—	—	—	19.334±0.239	kait2
2003gk 52937.237	—	—	—	—	—	19.784±0.265	kait2

Table A5 (cont'd)

SN	MJD	<i>B</i> (mag)	<i>V</i> (mag)	<i>R</i> (mag)	<i>I</i> (mag)	<i>Clear</i> (mag)	System
2006el 53965.324	—	—	—	—	19.808±0.464	kait3	
2006el 53972.281	—	—	—	—	18.153±0.250	kait3	
2006el 53973.007	18.866±0.068	18.366±0.050	18.050±0.086	17.825±0.126	—	nickel1	
2006el 53973.304	—	—	—	—	17.952±0.215	kait3	
2006el 53973.977	18.730±0.056	18.243±0.048	17.948±0.061	17.672±0.095	—	nickel1	
2006el 53974.304	—	—	—	—	17.865±0.175	kait3	
2006el 53981.255	—	—	—	—	17.328±0.140	kait3	
2006el 53993.265	—	—	—	—	17.563±0.215	kait3	
2006el 53993.957	18.990±0.089	18.169±0.180	17.600±0.269	17.334±0.314	—	nickel1	
2006el 53994.925	19.210±0.074	18.224±0.058	17.712±0.064	17.248±0.087	—	nickel1	
2006el 54001.269	—	—	—	—	17.888±0.183	kait3	
2006el 54021.156	—	—	—	—	18.561±0.462	kait3	
2006el 54028.887	20.665±0.141	19.613±0.078	18.937±0.056	18.110±0.057	—	nickel1	
2006el 54030.193	—	—	—	—	18.679±0.456	kait3	
2006el 54039.155	—	—	—	—	18.772±0.341	kait3	
2006el 54047.126	—	—	—	—	18.751±0.152	kait3	
2006el 54058.109	—	—	—	—	18.828±0.284	kait3	
2006el 54071.111	—	—	—	—	18.917±0.579	kait3	

This paper has been typeset from a $\text{\TeX}/\text{\LaTeX}$ file prepared by the author.